The Cell Division Role of Glypican 5 in Mammalian Cells

by

Ayşe Tuğçe Şahin

A Thesis Submitted to the
Graduate School of Sciences and Engineering

in Partial Fulfillment of the Requirements for

the Degree of Master of Science

in Molecular Biology and Genetics

August 2022

The Cell Division Role of Glypican 5 in Mammalian Cells

Koç University

Graduate School of Sciences and Engineering

This is to certify that I have examined this copy of a master's thesis

by

Ayşe Tuğçe Şahin

And have found that it is complete and satisfactory in all respects,

and that any and all revisions required by the final examining

committee have been made.

Committee Members:

_____

Assoc. Prof. Nurhan Özlü (Advisor, Koç University)

_____

Assist. Prof. Serkan Kır (Koç University)

_____

Assoc. Prof. Umut Şahin (Boğaziçi University)

Date: _____

This thesis is dedicated to my beloved family; Ulviye, Şaban, Gökçen, Erdem, Güneş and finally Patik…. I love you soo much!

ABSTRACT

The Cell Division Role of Glypican 5 in Mammalian Cells

Ayşe Tuğçe Şahin

Master of Science in Molecular Biology and Genetics

August 10, 2022

Glypicans (GPCs) are members of the Heparan Sulphate Proteoglycans (HSPGs) family of glycosaminoglycans. They are extracellular proteins anchored to the plasma membrane through their GPI anchor. Glypicans play role in developmental processes, cell differentiation, cancer progression, and stem cell function by regulating the activity of morphogens like Hedgehog and Wnt. An early RNAi screen has shown that the knockdown of Glypican 5 (GPC5) led to an increase in multinucleation suggesting a function in cell division. However, their role in cell division is not investigated. Our previous proximity dependent proteomic analysis in cytokinesis revealed that GPC5 interacts with proteins that are involved in cell adhesion, migration, actin reorganization, and RhoA activation. Even though cell division was extensively studied in terms of chromosome segregation and cytoskeleton dynamics, the function of cell surface proteins in cytokinesis remains elusive. In this thesis, I investigate the role of Glypican 5 in cell division by performing live cell imaging in GPC5 knock-out cells. In parallel, I investigated the functionality of previously identified interaction partners of GPC5. My analysis revealed that GPC5 have a role in the late cytokinesis by regulating adhesion properties of dividing cells specifically during abscission. This study illuminates the mechanism of how the outside and the inner part of the cell communicates during division.

ÖZETÇE

Memeli Hücrelerinde Glypican 5'in Hücre Bölünmesi Rolü

Ayşe Tuğçe Şahin

Yüksek Lisans, Moleküler Biyoloji ve Genetik

10 Ağustos 2022

Glypican'lar (GPC'ler), Heparan Sülfat Proteoglikanlar (HSPG'ler) glikozaminoglikan ailesinin üyeleridir. GPI çapaları aracılığıyla plazma zarına sabitlenmiş hücre dışı proteinlerdir. Glypican'lar, Hedgehog ve Wnt gibi morfojenlerin aktivitesini düzenleyerek gelişimsel süreçlerde, hücre farklılaşmasında, kanserin ilerlemesinde ve kök hücre fonksiyonunda rol oynar. Daha önce yapılan siRNA incelemesi, Glypican 5'in (GPC5) yıkılmasının, hücre bölünmesinde bir işlev öneren çoklu çekirdeklenmede bir artışa yol açtığını göstermiştir. Ancak hücre bölünmesindeki rolleri araştırılmamıştır. Sitokinezdeki önceki yakınlığa bağlı proteomik analizimiz, GPC5'in hücre yapışması, aktin yeniden organizasyonu ve RhoA aktivasyonunda yer alan proteinlerle etkileşime girdiğini ortaya koydu. Hücre bölünmesi, kromozom ayrımı ve hücre iskeleti dinamiği açısından kapsamlı bir şekilde çalışılmış olsa da, hücre yüzeyi proteinlerinin sitokinezdeki işlevi belirsizliğini koruyor. Bu tezde, GPC5 KO hücrelerde canlı hücre görüntülemesi yaparak Glypican 5'in hücre bölünmesindeki rolünü araştırıyorum. Buna paralel olarak, GPC5'in önceden tanımlanmış etkileşim ortaklarının işlevselliğini araştırdım. Analizim, GPC5'in özellikle absisyon sırasında bölünen hücrelerin yapışma özelliklerini düzenleyerek geç sitokinezde bir rolü olduğunu ortaya koydu. Bu çalışma, bölünme sırasında hücrenin dış ve iç kısmının nasıl iletişim kurduğunun mekanizmasını aydınlatmaktadır.

ACKNOWLEDGEMENTS

First and foremost, I would like to thank my supervisor Dr. Nurhan Özlü for the opportunity to work as a member of her team. I would also thank Dr. Nurhan Özlü, Dr. Nazan Saner and Prof. Ulrike Eggert for their guidance throughout my thesis project. In addition, I am grateful to Dr. Serkan Kır and Dr. Umut Şahin for accepting to be my jury member.

I acknowledge the Scientific and Technological Research Council of Turkey (TUBITAK) and Koç University for the financial and accommodational support during my graduate studies.

I am very thankful for the Proteomics Facility of Koç University, KUPAM, and especially Büşra Akarlar not just for the technical support but for her constant support, love and friendship! I also would like to thank each and every member of NOZLU group. To Dr. Aydanur Şentürk; thank you for everything you taught me about the proteomics and being a great work-friend. I am also grateful for the friendship that I have with Dr. Büşra Harmanda, I don't know how many times I told this, but you make everything bearable. To Berfu Nur Yiğit and Ceyda Seren Ceyhan; I had amazing time with both of you and thank you for your support during all the worst situation that we had encounter and all our discussions through last years. To Nazlı Ezgi Özkan Küçük; thank you for your friendship during my master studies. I would also express my gratitude to all the people I met at Koç University, especially the basement floor of Science Faculty. I am so grateful for all of you especially Hilal Dilşad Arabacı and Dila Gülensoy, we cried and laughed together side by side in the best and worst times.

To the Limonlu Coronalar; Ezgi Memiş, and Altuğ Kamacıoğlu (also former NOZLU lab members)! I am very thankful for both of your friendship and all the times we spent together. I am also grateful to both of you for the peoples that you bring to my life; Fat, Umut, Mali.

I feel so lucky to be existing in this school at the same time with the Koçtaşlar. Hüseen, thank you for your incredible and fun friendship. I would always be next to you even though we are living in different continents. Cancuu; my graduation buddy! I am looking forward to the years we will spend together and all the other finish lines. İdil the Dilek, sorry but I will always make you mad and have fun with it… Finally, to Beste a member of Limonlu Coronalar, Koçtaşlar, and lab, I am very grateful for your friendship, and I want you to know that I will always be in a phone call or a plane ticket away.

To my extended family, Selinay Şenkal, Serra Şener, Dilara Baş, Derya Garip, Nilsu Talaş, Gizem Sertkaya, Miray Şenkal, and Doğa Özder, I am the luckiest person in the world when it comes to you!

Finally, but the most importantly, I would like to thank to my family, who are my safety net; my mother Ulviye, my father Şaban, my sister Gökçen, Patik, and Güneş. You make everything more meaningful, and there are not enough words to describe my love to every single one of you.

TABLE OF CONTENTS

LIST OF TABLES

LIST OF FIGURES

ABBREVIATIONS

ABC Ammonium Bicarbonate

ACN Acetonitrile

ALIX ALG-2-interacting protein X

ANOVA Analysis of Variance

APC/C Anaphase Promoting Complex/Cyclosome

ATP Adenosine Triphosphate

BCA assay Bicinchoninic acid assay

BP Biotin-Phenol

BSA Bovine Serum Albumin

Cas9 CRISPR Associated Protein 9

CDK Cyclin Dependent Kinase

Cep55 Centrosomal Protein 55

Con A Concanavalin A

CRISPR Clustered Regularly Interspaced Palindromic Repeats

DAG1 Dystroglycan 1

DAPI 4',6-Diamidino-2-Phenylindole

DNA Deoxyribonucleic Acid

DMEM Dulbecco's Modified Eagle Medium

DMSO Dimethyl Sulfoxide

DTT Dithiothreitol

ECL Enhanced Chemiluminescence

ECM Extracellular Matrix

EGFP Enhanced Green Fluorescent Protein

ERK Extracellular Signal-Regulated Kinase

ESCRT Endosomal Sorting Complex Required for Transport

FBS Fetal Bovine Serum

G0 Resting State

G1 Gap 1

G2 Gap 2

GPC Glypican

GPC5 KO Hela Cas9 GPC5 sg2 with Doxycycline

GPI Glycosylphosphatidylinositol

GRGDSP synthetic linear RGD peptide**,** Gly-Arg-Gly-Asp-Ser-Pro

GPC5 KO Hela Cas9 GPC5 sg2 with Doxycycline

H2O2 Hydrogen Peroxide

HCl Hydrochloric Acid

HEK293T Human Embryonic Kidney 293 Cell Line

Hela WT Hela Cas9 GPC5 sg2 Doxycycline free

HRP Horseradish Peroxidase

HS Heparan Sulfate

HSPG Heparan Sulphate Proteoglycan

H_2O_2 Hydrogen Peroxide

ITGB1 Integrin B-1

ICB Intercellular Bridge

KCL Potassium Chloride

KO Knock-out

LB Liquid Broth Medium

HPLC High-Pressure Liquid Chromatography

HPSG Heparan Sulfate Proteoglycans

HRP Horse Radish Peroxide

myr-PALM myristoylation–palmitoylation

MS/MS Tandem Mass Spectrometry

NSCLC non-small cell lung cancer

PBS Phosphate Buffered Saline

PCR Polymerase Chain Reaction

pCMV-VSV-G

PEI Polyethyleneimine

PLL Poly-L-Lysine

RIPA Radioimmunoprecipitation Assay Buffer

ROBO1 Roundabout Guidance Receptor 1

RSK Ribosomal S6 Kinase

RT Room Temperature

SDS-PAGE Sodium Dodecyl Sulfate - Polyacrylamide Gel Electrophoresis

shRNA short hairpin Ribonucleic Acid

STC S-Trityl-L-cysteine

TBS Tris Buffered Saline

TCA Trichloroacetic Acid

UV Ultraviolet

VSP4 Vacuolar Protein Sorting 4-A

WT Wild type

Chapter 1:

INTRODUCTION

1.1. Cell Division and Its Regulation

The cell cycle, also known as cellular division, is the primary process involving DNA replication, followed by the subsequent segregation of the DNA copies into two daughter cells genetically identical to their parents (Schafer, 1998). These processes characterize the cell cycle's two significant stages: S and M phases. Chromosomal duplication occurs during the S phase of the cell cycle, which is also known as the phase for the synthesis of DNA in mammalian cells. This phase takes up roughly half of the cell cycle (Vermeulen, Van Bockstaele, & Berneman, 2003). Chromosomal segregation and cell division occur in the mitotic phase (M for mitosis), which comes immediately after the S phase and lasts longer than an hour. Mitosis and cytokinesis are the two fundamental processes during the cell cycle's M phase. Mitosis is the process by which copied chromosomes are distributed into a pair of daughter nuclei. At the same time, cytokinesis is the process by which the cell itself physically divides into two daughter cells (Hunt, Nasmyth, & Novák, 2011).

During the early phase of mitosis, specifically in the prophase, the two DNA molecules are gradually separated and condensed into pairs of sister chromatids held together by cohesion**.** Later in mitosis, as the nuclear envelope disassembles, the sister-chromatid pairs adhere to the mitotic spindle, a bipolar array of microtubules. In the metaphase stage, sister chromatids bind to opposite mitotic spindle poles and eventually align at the equator of the spindle. At the beginning of anaphase, with the loss of sister-chromatid cohesion, sister

chromatids start to separate from each other and then pull to opposing poles of the spindle (Civelekoglu-Scholey & Cimini, 2014). During telophase, the segregated chromosomes are packaged into separate nuclei after the spindle disassembly. Cytokinesis then divides the cell into two daughter cells, each inheriting one of each daughter nuclei (Ong & Torres, 2019).

Most cell cycles have gap phases—a G1 phase between the M phase and S phase and a G2 phase between the S phase and mitosis— in which cell growth occurs, and division occurs (Johnson & Walker, 1999). Consequently, the eukaryotic cell cycle consists of four main stages: G1, S, and G2, also known as interphase, and M (Pavletich, 1999).

In the G1 and G2 phases, the cell monitors the internal and external environment to ensure that conditions are favorable for initiating the S phase and mitosis. The G1 phase is particularly crucial in this regard. Its length is highly variable based on the microenvironment and extracellular signals coming from neighboring cells. If extracellular circumstances are favorable and growth and division signals are present, cells in early G1 or G0 pass through a checkpoint known as the restriction point near the end of G1. After reaching this threshold, cells are committed to the S phase, and DNA replication starts, even without external cues that encourage cell growth and division (Barnum & O'Connell, 2014).

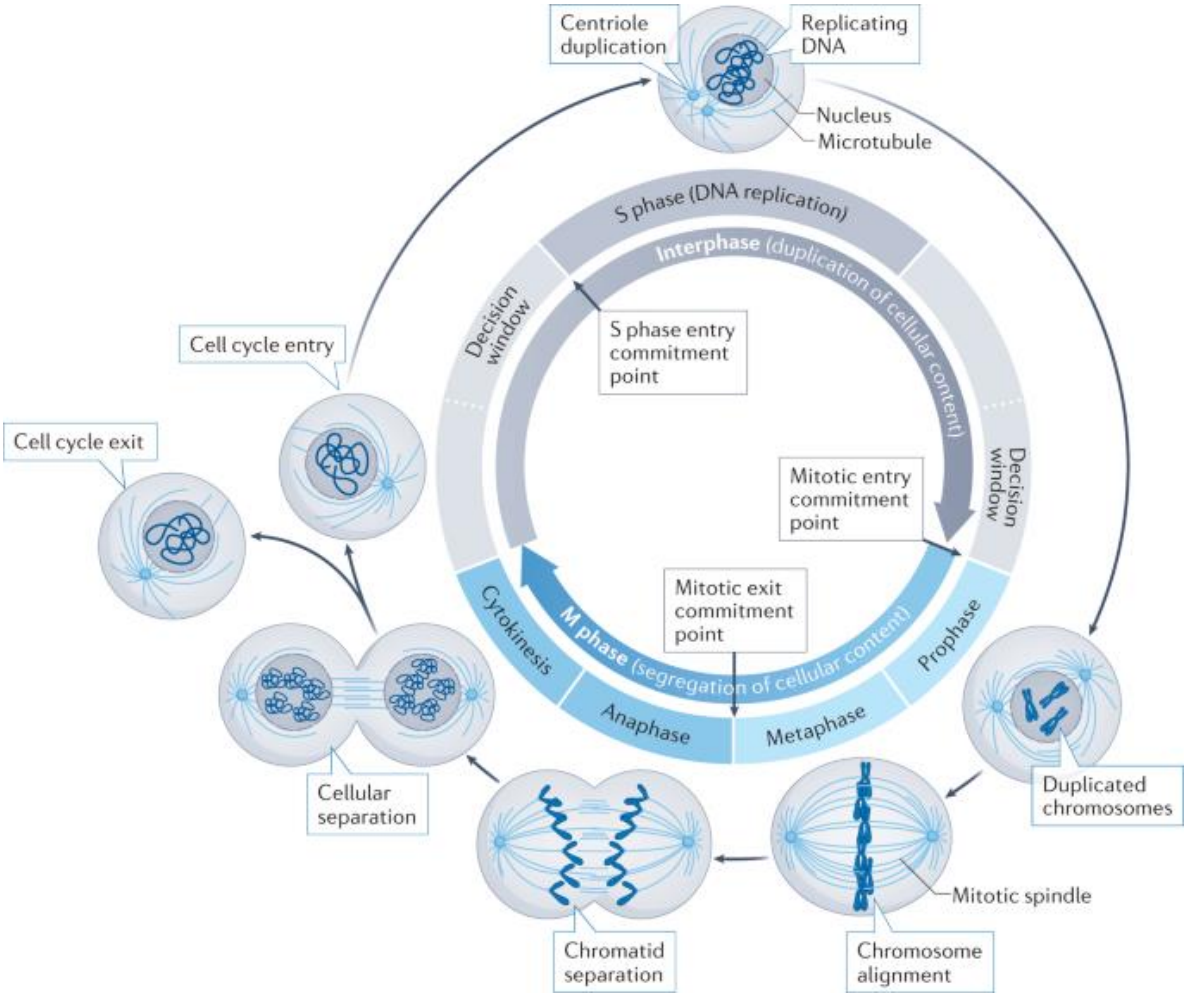

Figure 1.1.1: Overview of cell cycle and its regulators ((Matthews, Bertoli, & de Bruin, 2022)

The primary regulators of the cell cycle are the family of kinases called Cyclin-Dependent Kinase (CDK) and their activating proteins, cyclins. Throughout the cell cycle, cyclin levels fluctuate within the cell, but CDK levels remain steady. CDKs and cyclins are the primary mechanism major regulators of the cell cycle. Throughout the various cell cycle phases, the activity of several cyclin proteins and CDKs have a crucial role. While Cyclin D can activate CDK4 and 6 to trigger the G0/G1 transition, the activity of CDK2-Cyclin A complex and

their effector proteins regulates the S phase. The promotion of mitosis entry was regulated by the CDK1-Cyclin A complex, whereas the CDK1-Cyclin B complex monitors and controls mitosis (Ubersax et al., 2003). After the cell has passed the mitotic spindle checkpoint, the Cyclin A and B proteins are degraded by the Anaphase Promoting Complex/Cyclosome (APC/C) (Peters, 2006). Finally, cytokinesis is induced by this cascade of events with other kinases, phosphatases, and regulatory proteins.

1.2. Cytokinesis

The cell cycle ends with cytokinesis, splitting the plasma membrane between two nascent cells. Most cells go through mitosis and cytokinesis one after the other. Most animal cells start cytokinesis in anaphase and finish it soon after telophase (Pollard & O'Shaughnessy, 2019), and mammalian cytokinesis can be divided mainly into four stages (Figure 2.2).

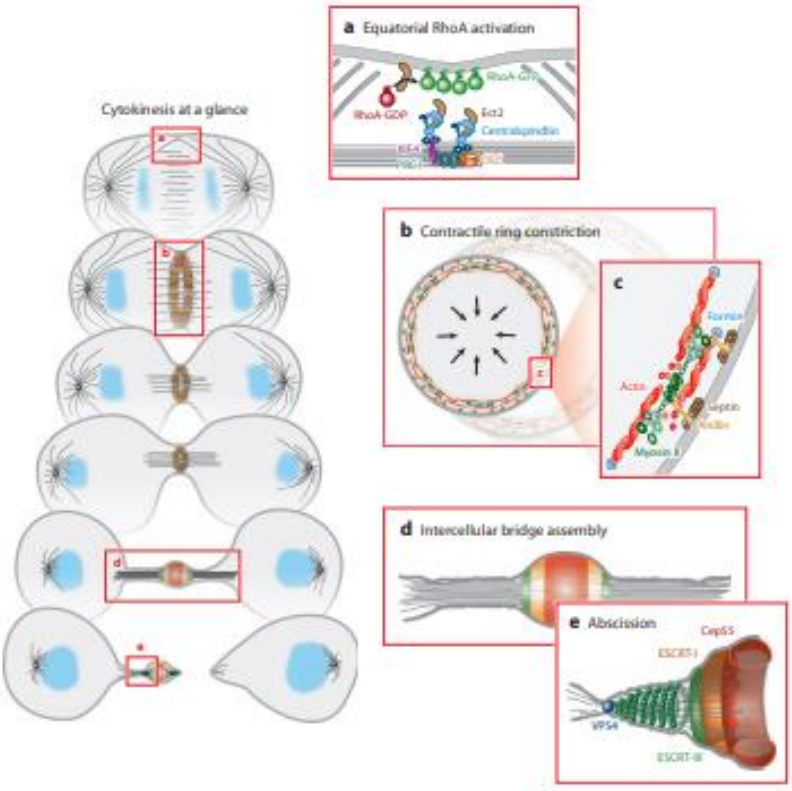

Figure 2.2. Four main stages of mammalian cytokinesis (Green, Paluch, & Oegema, 2012)

The four steps of cytokinesis are determining the cleavage site, the cleavage furrow ingression, the midbody's formation, and the cytokinetic abscission. Each stage depends on the previous stage; hence, any mistake or interference in any stage may cause cytokinesis failure (Mierzwa & Gerlich, 2014).

In the first stage of cytokinesis, the positioning of the cleavage plane occurs from a signal generated by the anaphase spindles (Bringmann & Hyman, 2005; Glotzer, 2005). Then, the central spindle, composed of microtubule bundles, recruits proteins necessary for the centralspindlin complex, such as Ect2, Kif4, and Rho-GEF. The centralspindlin complex proteins activate RhoA-GDP on the plasma membrane. After RhoA is activated, the

contractile ring assembles at the specified cleavage plane. If this phase is disrupted, cytokinesis cannot usually begin (Normand & King, 2010).

Through the assembly of a contractile ring and with the help of myosin-dependent motor activity, the ingression of cleavage furrow starts in the second stage of cytokinesis (Schroeder, 1972). Failure at this phase may result in a lack of furrow start or regression of the furrow (Carvalho, Desai, & Oegema, 2009).

The midbody and intercellular bridge formation is the third stage of cytokinesis (Mierzwa & Gerlich, 2014). In this stage, microtubules in the cleavage furrow increased even further until they reached 1-2 μm in diameter. At this stage, two daughter cells were connected to each other through a thin (1-2 micron) microtubule bundle called the intercellular bridge. Other components of centralspindlin like Kif4 and Prc1 are still associated with the microtubules in the center of ICB. A failure at this step will cause the cleavage furrow to regress (Lekomtsev et al., 2012).

1.2.1. Cytokinetic Abscission

Abscission, the last stage of cytokinesis, is where the width of the ICB even narrowed further (Guizetti et al., 2011; Pollard & O'Shaughnessy, 2019). This process requires functional midbody, so it depends on the successful third stage of the cytokinesis. During the abscission stages, a sequential constriction will happen in both sites of the midbody, microtubule bundles will compress, and this compression will result in the separation of 2 daughter cells and separate midbody (Guizetti et al., 2011). This process requires other proteins involved in vesicle transport and fusion like ESCRT proteins for constriction of the midbody. The midbody endures as a tether between two daughter cells. It is generally located in the middle of the intercellular bridge, a massive protein structure generated from antiparallel interpolar microtubule bundles (Iannantuono & Emery, 2021). Several abscission-associated proteins, including Cep55, ESCRT-I, and ALIX, are involved in the

recruitment of ESCRT-III to the midbody and the production of spiral polymers (McCullough, Colf, & Sundquist, 2013). There are several models for the mechanism of ESCRT-III mediated abscission at the midbody, like constriction during outgrowth and cut and slide. In the constriction during the outgrowth model, ESCRT-III spiral filaments perform the constriction of the membrane tube, and simultaneously, they grow away from the midbody (Guizetti et al., 2011). The cut and slide model explains the cytokinetic abscission as forming cylindrical spindles of ESCRT-III filaments next to the midbody and then splitting the filaments by VSP4 to release a fragment. The released ESCRT-III fragment will slide through the intercellular bridge while contrasting it and separating the two daughter cells (Elia, Fabrikant, Kozlov, & Lippincott-Schwartz, 2012). It was also shown that injuring the intercellular bridge with a laser triggers the accumulation of ESCRT-III and abscission (Lafaurie-Janvore et al., 2013). Based on these findings, it can be said that mechanical tension between two daughter cells may have an essential role in promoting successful abscission.

1.3. Cell adhesion changes through the cell cycle

The role and the regulation of adhesion in between the cell cycle transition is not yet clearly understood (Jones, Zha, & Humphries, 2019). As cells enter the S phase, the adhesion complex area and actin fibers increase. In dividing cells, specifically in G2 phase, the adhesion complexes diminishes while actin fibers disintegrate (Jones, Askari, Humphries, & Humphries, 2018). During this process, the variations in retraction forces in dividing cells correlate with the adhesion complexes' alterations (Vianay et al., 2018) and it was demonstrated that cellular tension is decreased in G2 a few hours before mitosis in epithelial cells (Uroz et al., 2018). It is known that cells undergo constantly remodeling their adhesion complexes during these stages (Jones et al., 2019).

The adhesion complexes and the cytoskeleton are interact with several proteins which have a crucial roles in cell division (Jones et al., 2019) (figure 2). As cell progress through the cell cycle, mitotic cell rounding and cytokinesis occurs with the RhoA activation and

contraction of contractile ring (Breznau, Semack, Higashi, & Miller, 2015; Glotzer, 2005; Maddox & Burridge, 2003). Another protein involved in the changes in adhesion complexes during cell cycle is formin. The activity of formin is very crucial for mitotic cells to be able to maintain the cortical actin (Ramanathan et al., 2015). Overall, all these roles of several proteins, changes in actomyosin complexes have an essential role in the regulation of the cell adhesion during cell cycle along with the spindle location and chromosome capture (Kunda, Pelling, Liu, & Baum, 2008).

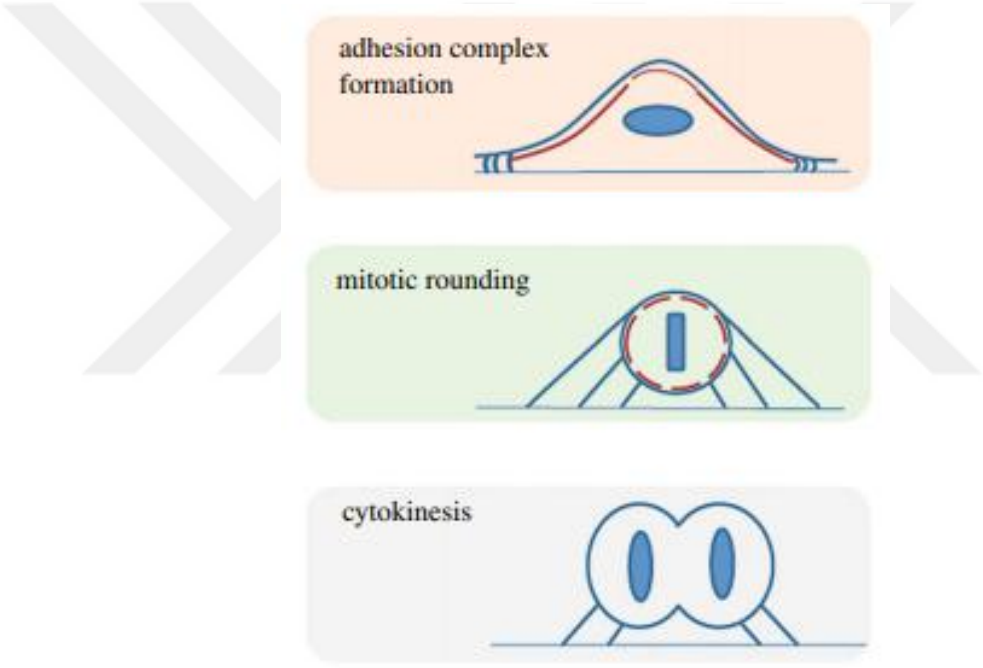

Figure 1.3.1: The changes in the adhesion through cell cycle (Jones et al., 2019)

Cells deconstruct adhesion complexes, round up, and begin mitosis after cyclin B1–CDK1 activation and nuclear translocation. Adhesion geometry before mitosis can affect spindle placement (Jones et al., 2018; Théry et al., 2005) and spatial memory (Théry & Bornens, 2008). Integrin-mediated adhesion is also critical for cytokinesis and daughter cell migration (Högnäs et al., 2012; Mathew et al., 2014; Pellinen et al., 2008; Taneja et al., 2016). These data support the idea that mitotic anchors maintain mitotic cells and provide a footprint

for dividing cells to build adhesion complexes that promote cytokinesis and the re-attachment of the nascent cell (Jones et al., 2019).

Some studies previously focused on mitotic cell adhesion using cells dividing on fibronectin. The localization of β1 integrins to the detached cell cortex in mitotic cells (Petridou & Skourides, 2016) and to the cleavage furrow in cytokinesis was demonstrated (Aszodi, Hunziker, Brakebusch, & Fässler, 2003; Pellinen et al., 2008; Reverte, Benware, Jones, & LaFlamme, 2006). It was also shown that β1 integrins influence cytokinesis while interacting with the ECM only in fibers that have not fully retracted (Dix et al., 2018).

In vitronectin- or culture-dish-attached cells, integrin αVβ5 mediates cell–ECM attachment (Lock et al., 2018). Integrin αVβ5 is present in two structures: classical focal adhesions with consensus adhesive components (Horton et al., 2015) and actin fibers and reticular adhesions (Lock et al., 2018). Reticular adhesions can mediate cell adhesions in the absence of talin and actin fibers. This finding supports there might be a new mechanism for attachment in mitosis

During mitotic cell rounding, αVβ5-containing structures remain connected with ECM at retraction fiber terminals and the attached surface of the cells. These complexes provide a mark for which daughter cells respread after cytokinesis. Interference of these adhesions causes abnormality in cell division due to alterations in mitotic spindle orientation, cytokinesis, and re-attachment (Lock et al., 2018). Altogether, integrins have a role in cell adhesion, even though their role in cell-cycle-dependent adhesion is not well understood.

1.3.1. Integrins and Their Role in Cytokinesis

Integrins are proteins with α-β subunits that act as adhesion receptors and bind extracellular matrix components. They are essential for adhesion-dependent cells to proceed through G1 and enter the S phase (Streuli, 2009). In recent studies there is increasing evidence supporting integrins also have a role in the regulation of cytokinesis (Aszodi et al.,

2003; Högnäs et al., 2012; Kittler et al., 2007; Thullberg, Gad, Le Guyader, & Strömblad, 2007). Nevertheless, the molecular mechanisms underlying integrin-regulated cytokinesis are yet poorly known.

In a study, integrins have a role in promoting cytokinesis by regulating ERK and RSK signaling. This study implies that integrins promote cytokinesis via modulating crucial abscission-required midbody processes (Mathew et al., 2014). They also demonstrate that adhesion-dependent and -independent pathways facilitate cytokinesis. In addition, several studies suggest that the correct interaction between cells and ECM components may help genomic stability by facilitating effective cytokinesis (Fujiwara et al., 2005; Galipeau et al., 1996; Lv et al., 2012).

More recently, it has been demonstrated that the interaction of Rab25 and integrin β1 regulates integrin trafficking and invasion in 3D matrix-grown epithelial cells (Caswell et al., 2007). In conjunction with Rab-dependent endosomal compartments, the spatially regulated activation of various kinases is required for integrin trafficking (Caswell & Norman, 2006). Recent evidence suggests that the ubiquitously expressed, small GTPase Rab21 associates with the tails of numerous integrins. Therefore, Rab21 is associated with regulating cell adhesion and migration by managing the trafficking of most integrin heterodimers (Pellinen et al., 2008). While the significance of integrin trafficking in migration is well understood, the role of integrin targeting in cell division is almost unknown.

Integrin signaling also has been linked with the control of cytokinetic abscission (Mathew et al., 2014; Sambandamoorthy et al., 2015). Analysis revealed that as cytokinesis nears completion, nascent cells migrate apart due to pulling forces on the intercellular bridge. It has been proposed that pulling forces might have a role in promoting abscission, possibly by decreasing the ICB width (Böttcher et al., 2009; Burton & Taylor, 1997). However, these pulling forces on the intercellular bridge can cause prolonged abscission (Lafaurie-Janvore et al., 2013). Forces play crucial but complex functions, possibly exerting opposing effects at various stages of abscission machinery assembly. Integrins have been linked to regulating cytokinesis in several cell types (Sambandamoorthy et al., 2015). Integrin β might regulate

cytokinesis through trafficking and its role in adhesion (Burridge & Chrzanowska-Wodnicka, 1996). Integrins might be crucial for understanding the effect of pulling forces in cytokinesis and its possible interactors.

Furthermore, the importance of mechanical inputs on abscission was shown. In fact, following the ingression, nascent cells produce nano Newton (nN) range pulling forces on the intercellular bridge, creating tension on ICB (Ariotti et al., 2014; Parton, Tillu, McMahon, & Collins, 2021). Instead of promoting abscission, the tension on ICB results in delays in ESCRT-III recruitment at the abscission site (Lafaurie-Janvore et al., 2013). Thus, it has been postulated that abscission requires a release in the tension created by the pulling forces on the ICB (Andrade et al., 2022; Lafaurie-Janvore et al., 2013), but it remains unclear how this is regulated. In a recent study, caveolae, known to regulate membrane tension in response to mechanical stress in interphase cells, are found at the midbody, abscission site, and between ICB and cell interface. They demonstrated that the absence of caveolae interferes with the recruitment of ESCRT--III during cytokinesis and delays the abscission.

1.4.Glypicans

Glypicans, also known as GPCs, are members of the Heparan Sulphate Proteoglycans (HSPGs) family of glycosaminoglycans (N. Li, Gao, Zhang, & Ho, 2018). This family is highly conserved across all eukaryotic species. They are mostly located on the outside of the plasma membrane, which is also where they covalently attach to the membrane using GPI anchors. GPC1-GPC6 are the names of the six different proteins that make up the Glypican family. There are two subfamilies that can be used to classify glypicans: GPC1/2/4/6 and GPC3-5. The orthologs of the GPC 1-2-4-6 and GPC 3-5 genes also found in the fruit flies are Dally and Dlp (Dally-like protein).

Every glypican carries both a putative C-terminal sequence and an N-terminal secretory signal sequence. Both sequences are required for GPI anchor attachment. It is believed that glypicans have a similar three-dimensional structure due to the existence of seven disulfate bridges that are generated by fourteen cysteine residues that are conserved

(N. Li, Spetz, & Ho, 2020). In addition, each of the six Glypican members carries a conserved location for the attachment of glycosaminoglycan (GAG) chains close to the place where they bind to the membrane. These motifs are required for Heparan Sulfate (HS) attachments to take place (Song & Filmus, 2002).

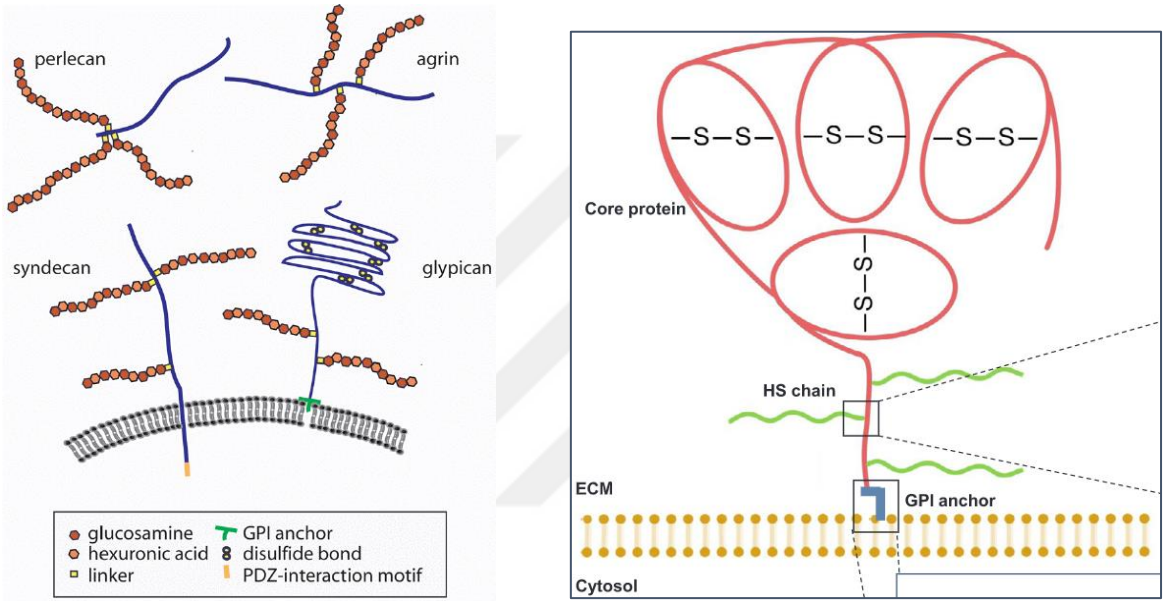

Figure 1.4.1: Structure of HPSG and Glypicans

Some glypicans may be cleaved proteolytically by Furin-like convertases, which may result in the generation of two subunits that remain attached to one another through disulfide bridges. Alternatively, some glypicans may cleave by the lipase Notum and be released into the extracellular space (Capurro, Shi, Izumikawa, Kitagawa, & Filmus, 2015; Fico, Maina, & Dono, 2011; Filmus & Capurro, 2014; Traister, Shi, & Filmus, 2008).

Glypicans have a diverse array of modifications on their HS chains, which is the primary reason (but not the only reason) for their interactions with a wide variety of chemicals and proteins. They have a role in the regulation of developmental processes, tissue reorganization, and cellular differentiation, along with many signaling pathways, due to the

fact that they are located and interact with the microenvironment (Kaur & Cummings, 2019; N. Li et al., 2020). This allows them to interact with growth factors, extracellular matrix proteins, cytokines, and chemokines, which in turn causes them to regulate these processes.

Glypicans have been proven to be involved in a wide variety of malignancies and other disorders because of their extensive ligand repertoire. Glypicans are able to perform the dual role of tumor suppressors and oncogenes due to the diverse ways in which they are expressed in the many distinct types of cancer. This dual activity of glypicans is mainly dependent not only on the type of cancer cells but also on the disease level (Fico et al., 2011; Kaur & Cummings, 2019; N. Li et al., 2020; Nishida & Kataoka, 2019; Song & Filmus, 2002)

1.4.1. Glypican 5

The GPC5 gene is in the 13q31.3 region of the genome, which is 1.47 Mb wide (Veugelers et al., 1997). Glypican 5 is a 572 amino acid protein with five predicted Heparan Sulfate attachment sites at S441, S486, S495, S507, and S509 near its C terminus. It is found that GPC5 regulates the kidney, brain, and limb in the developing embryos(Saunders, Paine-Saunders, & Lander, 1997). In adults, the central nervous system has a lot of GPC5 expressions (Kaur & Cummings, 2019; Veugelers et al., 1997).

It was shown that GPC5 is associated with different kinds of diseases like rhabdomyosarcoma. Two studies show that GPC5 mRNA levels are higher in rhabdomyosarcoma (RMS) because the GPC5 gene is amplified (N. Li et al., 2020; Nishimura et al., 2013). This suggests that GPC5 expression might be a reason for cancer in RMS. Also, salivary adenoid cystic carcinoma that spreads to the lungs has shown that GPC5 can cause cancer (Y. Zhang, Wang, Dong, Li, & Hou, 2014). In other studies, a single-polypeptide polymorphism in the GPC5 gene may make people more likely to get lung cancer (Y. Li et al., 2010; Yang et al., 2013). In another study, GPC5 expression was found to be lower in non-small cell lung cancer (NSCLC), and when GPC5 was overexpressed in these cells, they lost their metastatic ability (Yang et al., 2013). Another study showed that GPC5

is an epigenetically silenced protein that acts as a tumor suppressor NSCLC by inhibiting the Wnt signaling (Yuan et al., 2016). Overall, several studies showed that GPC5 expression is reduced in different cancer types like prostate, breast, glioma, and pancreatic cancer (Hong et al., 2019; C. Zhang et al., 2016; C. Zhang et al., 2011).

Altogether, GPC5 is an extracellular protein that has numerous roles and effects on different diseases. All these findings support that GPC5 might have a role in cancer proliferation and progression with several interactions. Since it is an extracellular protein, it might interact with various proteins, which may be necessary to regulate cancer proliferation and migration. To this end, in the thesis, we were focused on the role of Glypican 5 during cell division, specifically cytokinetic abscission.

Chapter 2:

MATERIALS AND METHODS

2.1. Cell culture conditions and synchronization methods

Dulbecco's Minimum Essential Medium with 10% FBS (Fetal Bovine Serum) and 1% Penicillin/Streptomycin was used for Hela Kyoto cells, while for Doxycycline inducible HelaCas9 GPC5 sg2 cells were grown Dulbecco's Minimum Essential Medium with 10% tetracycline-free FBS (631367, Takara) and 1% Penicillin/Streptomycin in 37℃ incubator with 5% CO2.

For the synchronization of the cells, a single thymidine treatment was done and followed by approximately around 8 to 10 hours of release time to observe mostly cytokinetic cells in the population. As another method, monopolar synchronization was performed after double thymidine treatment by treating the cells with 10 μM STC (164739, Sigma- Aldrich) in complete DMEM for 12 hours, followed by 15 minutes treatment of 100M Purvanol A (1580, Tocris Bioscience).

2.2. Live cell imaging

2.2.1. Laminin coating for live cell imaging

Firstly, one 8-well chamber slide (Ibıdı, 80826) was coated using 10 μg/ml Laminin (Santa Cruz, 631105) at 37℃ for an hour. Then, laminin was removed from the dishes, and wells

were washed with 1X PBS gently. Then cells were seeded with 10% confluency using Tet-free complete DMEM, and the GPC5 KO cells were introduced to Doxycycline with a final concentration of 1 μg/μl. After 48 hours, brightfield live cell imaging was done for 12 hours, and images were taken every 3 minutes.

2.2.2. Live cell imaging using 1 mM GRGDSP

Cells were seeded in 8-well chamber slides (Ibıdı, 80826) with 10% using Tet-free complete DMEM, and the GPC5 KO cells were introduced to Doxycycline with a final concentration of 1 μg/μl. After cell seeding, cells were incubated in a 37℃ incubator with 5% CO2 for 48 hours. Prior to the brightfield live cell imaging, cyclo-GRGDSP peptide (Anaspec, AS-61110) were applied to both HelaCas9 WT and GPC5 KO cells with a final concentration of 0.5 mM. Live cell imaging was done for 12 hours, and images were taken every 3 minutes.

2.3. Coating of the coverslips

The coverslips were placed in a 24-well plate and sterilized with UV for 10 minutes. Then, coverslips were coated with Concanavalin A from *Canavalia ensiformis* (Sigma Aldrich, C5275), Laminin (Santa Cruz, 631105), and Poly-L-Lysine Hydrobromide (Sigma Life Sciences, Cat. #P9155).

2.3.1. Concanavalin A coating

After UV sterilization, 0.5 mg/ml working solution of the Con A was prepared using sterile water. 0.5 mg/ml solution was applied to the coverslips and waited another 10 seconds. After 10 seconds, the excess Con A was discarded carefully without harming the surface of the coverslips. Plates were dried for around 15 to 30 minutes at room temperature.

2.3.2. Laminin coating

10 µg/ml Laminin solution was prepared from 1mg stock solution. Then, 10 µg/ml laminin was added to coverslips and incubated at 37℃ for at least 1 hour. After incubation, excess laminin was discarded, and plates were stored at 4℃.

2.3.3. Poly-L-Lysine coating

50 µg/ml working solution was prepared using 1X PBS from 2 mg/ml stock solution. The coverslips were treated with the 50 µg/ml working solution and incubated at 37℃ overnight. The next day, excess PLL was removed, and coverslips were washed with sterile water three times. Before cell seeding, coverslips were dried entirely under a laminar hood.

2.4. Proximity-dependent HRP-based biotinylation and pulldown using streptavidin beads

HEK293T cells were cultured in 150 mm culture plates with a confluence of 60%. Prior to transfection, the medium was switched to transfection enhancement media (DMEM with 1% FBS, without antibiotics). In a another eppendorf tube, 1 ml Opti-MEM was combined with 40 µg of cMyc-HRP-GPC5 in pLenti CMV Hygro DEST. The DNA was further diluted with 120 µl of PEI (1 mg/ml) and the mixture was vortex immediately. Then, the mixtures were incubated for 20 minutes at RT. DNA/PEI mixture were applied drop by drop to the cells (20 ug DNA per plate) and cells were cultured at 37℃ in an incubator with 5% CO2. The next day, the transfection enhancement medium was substituted with complete DMEM (10% FBS, 1% P/S).

After 48 hours, one plate of cMyc-HRP-GPC5 transfected HEK293T cells and one plate of HA-HRP-GPC3 transfected HEK293T cells were labelled in 15 ml of complete medium supplemented with 500 µM Biotin-Phenol (LS-3500.1000, Iris Biotech GMBH) and 1mM H2O2 for 1 minute at room temperature. After a 1-minute incubation, labeling solution was

rapidly aspirated and washed three times with a quencher solution containing 10mM Sodium L-Ascorbate (11140, Sigma Aldrich), 5 mM Trolox (6-hydroxy-2,5,7,8-tetramethylchroman-2-carboxylic acid,) (238813, Sigma Aldrich), and 10mM Sodium Azide (BP9221, Fisher Scientific). Similarly, the other two plates (control plates) were incubated for 1 minute at room temperature in 15 ml of complete medium supplemented with 1 mM H2O2 and then washed three times with quencher solution. The cells at the bottom of the plates were scraped using 5 ml of quencher solution. The cells were collected in falcon tubes and pelleted by centrifugation at 4℃ at 1000 rpm for five minutes. The supernatants were collected, and the cells were placed on ice in preparation for lysis. In 125 µl RIPA lysis buffer supplemented with 100X Protease Inhibitor and quenchers; cells were resuspended. Following the manufacturer's instructions, lysates were collected, and protein concentrations were determined using the BCA protein assay kit (23227, Pierce). 1 mg of lysates was loaded onto 150 µl aliquots of streptavidin beads (Pierce Streptavidin UltraLink Resin, 53117) that had been prewashed twice with 1 ml of RIPA lysis buffer and equilibrated at room temperature. On a rotator, the samples were incubated overnight at 4°C.

The following day, beads were pelleted by centrifugation at 1000 rpm for 5 minutes. Beads were washed with RIPA lysis buffer twice, 1 M KCl, 0.1 M Na2CO3, 2 M urea in 10 mM Tris-HCl (pH 8.0), and RIPA lysis buffer twice. Then beads were washed again twice with 100 mM Tris-HCl (pH 8.5) and twice with 8 M Urea in 100 mM Tris-HCl (pH 8.5) for LC-MS/MS protein identification. The beads were shaken in urea solution supplemented with 100 mM DTT for 30 minutes at 1000 rpm and 56℃ before being rinsed with again in urea solution. The beads were then shaken in a 50 mM 2-chloroacetamide in urea solution for 20 minutes at 1000 rpm and 25℃. The samples were washed 4 times in urea solution and 4 times in 50 mM Ammonium Bicarbonate (ABC) solution in HPLC grade water. After washing, Trypsin (PierceTM Trypsin Protease, MS Grade, PI-90057) in 1 mM HCl was diluted 1:150 (µg of Trypsin: µg of WCL) and added to beads for on-bead digestion. After 10 minutes of incubation on ice, 500 µl of ABC solution was added, and beads were shaken overnight at 1000 rpm at 37℃. The following day, the beads were centrifuged at 1,000 rpm

for five minutes, and the supernatants (peptides) were collected in a new tube. 10 % formic acid was added to the beads until the final concentration reached 1 % (1:10 dilution) until the pH of the samples reached 2-3. The peptides were dried using speed-vac.

For sample purification, Stage tips were packed using 3 discs of C18. To condition the stage tips, 60 µl of methanol and 60 µl of Buffer A (0.5% Formic Acid in 5% ACN) were loaded and spun for 10 minutes at 2500 rpm, respectively. Peptides were resuspended in 60 µl Buffer A (0.5% Formic Acid in 5% ACN) and sonicated for 2 minutes to ensure full resuspension of peptides. The samples were passed through the stage tips. Flow through was discharged, stage tips were washed with 60 µl Buffer A using centrifuge for 10 minutes at 2500 rpm. Lastly, the peptides were eluted by adding 60 µl of Buffer B (0.1% Formic Acid in 70% ACN) at 3000 rpm for 15 minutes using bench-top centrifuge. The samples were dried in speed vacuum before LC-MS/MS analysis.

All samples were run using C18 nanoflow reversed-phase HPLC coupled with Thermo Scientific Q-Exactive Orbitrap mass spectrometer. The data sets were searched against the UniProt for humans using Proteome Discoverer 2.3. Using the STRING v.11 database network maps of interactomes were revealed, and gProfiler was the tool that used to analyze the GO cellular component annotations. The network of protein interactions was visualized with Cytoscape 3.8.1.

* Ezgi Memiş and Altuğ Kamacıoğlu conducted the initial experiments and analysis of the protein lists.

2.5. Cloning of DAG1, and ROBO1 shRNA oligos into pLKO.1 TRC cloning vector

For the generation of scramble, DAG1 and shROBO1 shRNA constructs were cloned into pLKO.1 TRC cloning vector (Addgene, Plasmid #24150) plasmids. Three shRNA sequences against DAG1 and ROBO1, and one scramble shRNA were ordered from Sigma-

Aldrich. Table 3.3.1 shows the forward and reverse oligo sequences. pLKO.1 TRC cloning vector was digested with AgeI and EcoRI for 3 hours at 37 °C using Cut Smart buffer. Digested vector was run on 1% low melting point agarose gel at 100V for 45 minutes. 2 distinctly separated bands were observed in the size of 7 kb and 24 bp. 7kb band were cut out and DNA was purified using NucleoSpin Gel and PCR Clean-up Kit Kit (740609, Macharey-Nagel) following manufacturer's instructions.

Before annealing, forward and reverse oligos were resuspended in ddH_2O to a concentration of 20 μM. First, resuspended 20 μM forward and reverse oligos were mixed in 1:1 ratio in the presence of 10X NEB Buffer 2 and ddH_2O. Oligo mix were incubated for 5 minutes at 95 °C in a beaker of boiling water. Then, beaker was cooled down to room temperature slowly for the annealing of the oligos. For the ligation of the annealed oligos with the digested pLKO.1 TRC cloning vector, annealed oligos were mixed with digested vector, T4 DNA ligase buffer, T4 ligase and ddH_2O. Ligation mix was incubated at 16 °C for 16 hours in PCR machine.

Table 2.5.1: shRNA sequences targeting potential interaction partners of GPC5 during cytokinesis

Scramble	**sh1**	**Forward oligo**	CCGGCCTAAGGTTAAGTCGCCCTCGGGATCCCGAGGGCGACTTAACCTTAGGTTTTTG
		Reverse oligo	AATTCAAAAACCTAAGGTTAAGTCGCCCTCGGGATCCCGAGGGCGACTTAACCTTAGG
DAG1	**sh1**	**Forward oligo**	CCGGCGAGTGACCATTCCAACAGATGGATCCATCTGTTGGAATGGTCACTCGTTTTTG
		Reverse oligo	AATTCAAAAACGAGTGACCATTCCAACAGATGGATCCATCTGTTGGAATGGTCACTCG
	sh2	**Forward oligo**	CCGGCGGTGGTGAATAACAGACTATGGATCCATAGTCTGTTATTCACCACCGTTTTTG
		Reverse oligo	AATTCAAAAACGGTGGTGAATAACAGACTATGGATCCATAGTCTGTTATTCACCACCG
	sh3	**Forward oligo**	CCGGTTGTCGGCACCTACAGTTTATGGATCCATAAACTGTAGGTGCCGACAATTTTTG
		Reverse oligo	AATTCAAAAATTGTCGGCACCTACAGTTTATGGATCCATAAACTGTAGGTGCCGACAA
ROBO1	**sh1**	**Forward oligo**	CCGGTGACACATGACGCCAGATAAAGGATCCTTTATCTGGCGTCATGTGTCATTTTTTG
		Reverse oligo	AATTCAAAAATGACACATGACGCCAGATAAAGGATCCTTTATCTGGCGTCATGTGTCA
	sh2	**Forward oligo**	CCGGATAGCGAAGAGTACAACATTTGGATCCAAATGTTGTACTCTTCGCTATTTTTTG
		Reverse oligo	AATTCAAAAAATAGCGAAGAGTACAACATTTGGATCCAAATGTTGTACTCTTCGCTAT
	sh3	**Forward oligo**	CCGGTTGCTGCCGAGTGGATCTTTAGGATCCTAAAGATCCACTCGGCAGCAATTTTTG
		Reverse oligo	AATTCAAAAATTGCTGCCGAGTGGATCTTTAGGATCCTAAAGATCCACTCGGCAGCAA

For the transformation chemically competent *E.coli* stbl3 bacteria were prepared using 10X transformation buffer containing 100 mM HEPES (pH 6.7), 150 mM $CaCl_2$, 550 mM $MnCl_2$ and 2.5 M KCl according to Christian Hoerner's preparation protocol (version 1.3). 5 µl ligation product were mixed with 50 µl competent *E.coli* stbl3 and incubated for 30

minutes on ice. Then for 45 seconds, heat shock was applied at 42°C. Following the heat shock, competent *E.coli* stbl3 and ligation product mixed were incubated on ice for 2 minutes. Then, 450 µl pre-heated LB were added to the mix and incubated at 37 °C for 1 hour at 900 rpm on shaker. After 1 hour incubation, mixture was plated onto ampicillin containing Agar plates and incubated for 16 hours at 37 °C. In the following day, colonies were selected from the plate and inoculated in liquid broth containing ampicillin and incubated at for 16 hours at 37 °C. Then, bacteria culture was centrifuged and plasmid DNA extraction from the pellet was done using NucleoSpin Plasmid DNA mini kit according to the manufacturer's instructions. Purified plasmids were confirmed with the digestion of the plasmid using BamHI enzyme and sequenced with pLKO forward primer 5'- CAA GGC TGT TAG AGA GAT AAT TGG A- 3' by Macrogen Company. After these confirmations, plasmids were used in the following experiments.

2.6. Virus packaging of constructed pLKO.1 TRC plasmids

The HEK293T cell line was used for lentiviral plasmid packaging. One day before the transfection, cells were planted on 6 cm cell culture plates to be 25 percent confluent. Following day, cells were transfected as follows: 1000 ng transfer plasmid, 1000 ng psPAX2, and 100 ng pCMV-VSV-G were combined in 90 µl Opti-MEM (31985062, Thermo Fisher Scientific). In a separate Eppendorf tube, 93 µl Opti-MEM and 7 µl FuGene transfection reagent (Promega E2311) were combined and incubated at room temperature for 5 minutes. Then, the plasmid mixture was added drop by drop to the transfection reagent solution and stirred gently. The final mixture was incubated for 30 minutes at room temperature before being dripped directly onto the cells. By gently shaking the cell culture plate, the transfection mixture was equally disseminated throughout the media for cell growth. Next morning, 3 ml of fresh complete DMEM was used to replace the transfection medium. At 48 hours post-

transfection, the first viral supernatant was extracted and kept at 4 °C. Again, 3 ml of fresh media for cell development was added to the cells. The second viral supernatant was collected

72 hours after transfection and combined with the first. After bleach sterilization, packaging cells were thrown away. The viral supernatant was filtered through a 0.45 μm membrane and 1 ml was aliquoted into Eppendorf tubes and stored at -80 °C for long-term preservation.

2.7. Transfection and lentiviral transduction

In order to carry out transfection, cells were seeded with the goal of reaching a confluency of sixty percent on the day of the procedure. The following day, the cells were given two washes in PBS, after which Transfection Enhancement Medium (DMEM containing 1% FBS and 1% PS) was added. The cells were then placed in an incubator at 37 degrees Celsius with 5% carbon dioxide for half an hour. In the meantime, to transfect 1 ug of DNA, 1 μl of Lipofectamine^{TM} 2000 Transfection Reagent (11668019, Invitrogen) and 1 ug of DNA were individually diluted in 80 μl of OPTI-MEM (31985047, Invitrogen) in 1.5 ml test tubes. This was done such that the final concentration of each was 80 ul. Incubation took place for a period of five minutes at a temperature of room temperature. The DNA that had been diluted and the Lipofectamine^{TM} 2000 that had also been diluted were combined in a fresh tube at a ratio of 1:1, gently mixed by tapping, and then allowed to incubate at room temperature for twenty minutes. The concoction was drizzled onto the cells in a very careful manner. After a period of six hours, the transfection media were changed out for fresh complete DMEM.

For the generation of Doxycycline inducible CRISPR GPC5 KO cells, the guide RNAs that Dr. Federico Donà (Eggert Group at King's College London) designed were used. Hela Cas9 cells that had been obtained from the Cheeseman Group at MIT and were engineered to stably express Cas9 were transfected with GPC5 sg2 lentiGuide-Puro (Addgene #52963). Following a transduction period of 48 hours, the cells were chosen using puromycin at a concentration of 2 g/mL.

Hela Cas9 GPC5 sg2 cells which are stably expressing DAG1 and ROBO1 shRNAs were created with the help of lentiviral transduction. Hela Cas9 GPC5 sg2 cells were seeded in a 6-well plate for the purpose of transduction, and 500 μl of virus was added to each well. To

boost transduction efficiency protamine sulfate was used as an adjuvant and two consecutive transductions were conducted. Protamine sulfate (P4020, Sigma-Aldrich) was prepared as an 8 mg/ml stock solution in water and utilized at a final concentration of 8 ug/ml for transduction.

On day 1, the first transduction of cells was conducted. On day three, the first transduction medium was eliminated, and a second viral transduction was carried out as on day one. Hygromycin was utilized at a final concentration of 400 μg/ml in growth media for 10 days to select transduced cells, while all control cells died under hygromycin selection.

2.8. Western blotting

Cell pellets were lysed in 1X PBS buffer with 0.1 percent TritonX- 100, Complete EDTA-free protease inhibitor cocktail (Roche), and PhosSTOP phosphatase inhibitor mixture (Roche). 1 tablet of inhibitor cocktail was added to 10 ml of lysis buffer. By pulling the cell suspension through a thin syringe, the cells were disrupted. The cell debris was eliminated by centrifugation at 14,000 rpm for 5 minutes at 4 °C. Using a BCA protein assay kit, protein concentration was determined (23227, Pierce). Protein samples were mixed with 2X Laemmli sample buffer containing 4 percent (w/v) SDS, 20 percent glycerol, 120 mM Tris-Cl (pH 6.8), 0.02 % (w/v) bromophenol blue and 100 mM dithiothreitol (DTT) in a 1:2 (v/v) ratio of protein sample to final volume of the sample. The samples were heated at 95°C for 5 minutes for denaturation before being cooled and loaded onto SDS-PAGE gel. For the separation of proteins, 10% and 12% SDS-PAGE gels were utilized. After 100 minutes of electrophoresis at 120 V, the XCell II Blot Module (ThermoFisher-Scientific) was used to transferred proteins to nitrocellulose membranes (BA85, Whatman Protran). After 45 minutes of blocking with 3% milk in 1X TBS-Tween 20 Buffer, the membrane was incubated overnight at 4°C or for 3 hours at room temperature with the primary antibodies listed in Table 3.6.1. The membrane was washed three times for 5 minutes with 1X TBS-Tween 20 Buffer and then incubated at room temperature for 1.5 hours with the secondary antibodies

listed in Table 3.6.2. Finally, membranes were washed three times for 5 minutes with 1X TBS-Tween 20 Buffer, and proteins were visualized using Clarity Western ECL Substrate (1705060) using The ChemiDoc MP Imaging System (Bio-Rad).

Table 2.8.1: Antibodies and dilutions for western blotting

Antibody	Host	Dilution	Brand	Cat number
Recombinant Anti-Integrin β1	Rabbit	1:2000	Abcam	ab52971
Anti-DAG1	Mouse	1:1000	Abcam	ab234587
Anti- ROBO1	Rabbit	1:500	Abcam	ab7279
Alpha-Tubulin (DM1A)	Mouse	1:1000	Cell Signaling	3873S
Anti-Rabbit IgG-HRP	Goat	1:2000	Cell Signaling	7074S
Anti-Mouse IgG-HRP	Horse	1:2000	Cell Signaling	7076S

2.9. Immunofluorescence staining

For immunostaining, glass coverslip-seeded cells were fixed for 15 minutes in 3.2 percent paraformaldehyde in 1X PBS. Three times for three minutes, coverslips were washed with TBS-0.1 percent Triton X-100 Buffer. After 45 minutes of blocking with 2% BSA in TBS-0.1% Triton X-100, coverslips were incubated with primary antibodies in 2% BSA in TBS-0.1% Triton X-100 at 4°C overnight or at room temperature for 3 hours. The coverslips were then rinsed three times for three minutes with TBS-0.1% Triton X-100 Buffer and incubated for 1.5 hours at room temperature with secondary antibodies. Following washing, coverslips were incubated with 1:500 DAPI in 2% BSA in TBS-0.1% Triton X-100 for 15 minutes. Coverslips were imbedded in Mowiol® mounting media (81381-Sigma-Aldrich) and sealed with nail polish on microscope slides following the final washing procedure.

Table 2.9.1. Antibodies and dilutions used for immunostaining

Antibody	Host	Dilution	Brand	Cat number
Recombinant Anti-Integrin β1	Rabbit		Abcam	ab52971
Anti-DAG1	Mouse		Abcam	ab234587
Anti- ROBO1	Rabbit		Abcam	ab7279
Alpha-Tubulin (DM1A)	Mouse		Cell Signaling	3873S
Tubulin	Rat	1:100	Abcam	Ab6160
Anti-PLK	Mouse		Santa-Cruz	Sc-17783
Phalloidin-iFlour	-	1:5000	Abcam	Ab17656
Anti-mouse IgG Alexa Flour (H+L) 488	Donkey	1:1000	Life Technologies	A21202
Anti-Rabbit IgG (H+L) Dylight 488	Goat	1:1000	Thermo Scientific	35552
Anti-mouse IgG (H+L) Alexa Fluor 633 Aliquot	Goat	1:1000	Life Technologies	A21052
Anti-rat IgG (H+L) Alexa Fluor 568	Goat	1:1000	Life Technologies	A11077
Anti-rabbit IgG Alexa Flour (R) 555 Fab2	Goat	1:1000	Cell Signaling	4413S

2.10. Microscopy and quantification

All images of fixed samples were collected using the Inverted DMI8 SP8 Confocal Microscope with the help of 2 PMT, 2 HyD, 1 TLD (PMT Trans) detectors and 10x / 0.30 DRY (HC PL FLUOTAR), 20x / 0.55 DRY (HC PL FLUOTAR), 40x / 1.30 OIL (HC PL APO CS2), 63x / 1.40 OIL (HC PL APO CS2) objectives. For the orthogonal views of the

cells, the images of the cells were taken in each 0.5 micron. Orthogonal views of the cells were employed using ImageJ. For brightfield live imaging of cells, a Leica DMi8 equipped with HC PL FL L 20x/0.40 CORR and HC PL APO 63x/1.40-0.60 OIL objectives was used, and 5 Z stack were taken throughout the cell. All quantification and representation of the cells were done using ImageJ.

For significance analysis, an unpaired, two-tailed Student's t-test, two-way ANOVA was applied. GraphPad Prism version 9.00 for Windows, GraphPad Software, La Jolla, California, USA, www.graphpad.com, was used to construct all super plots.

Chapter 3:

RESULTS

3.1. GPC5 enrich in between two daughter cells during cytokinesis.

EGFP-tagged constructs in pLenti plasmids of GPC5 were used to comprehend the spatiotemporal localization of GPC5 during cell division. These constructs were transfected using Lipofectamine into HeLa Kyoto cells and visualized using live cell imaging.

It was seen that GPC5 (Figure 4.1.) relocate to the cell membrane during metaphase and anaphase, with no detectable membrane enrichment GPC5 are enriched along the cleavage furrow during early telophase. The enrichment of both proteins at the cleavage furrow increases throughout mid-telophase and reaches a maximum during late telophase.Using myr-PALM-GFP as controls, GFP-GPC5 (Figure 4.1) signals near the cleavage furrow at mid-telophase have increased significantly. Therefore, GPC5 enriches significantly in between the two nascent cells during cytokinesis cell division.

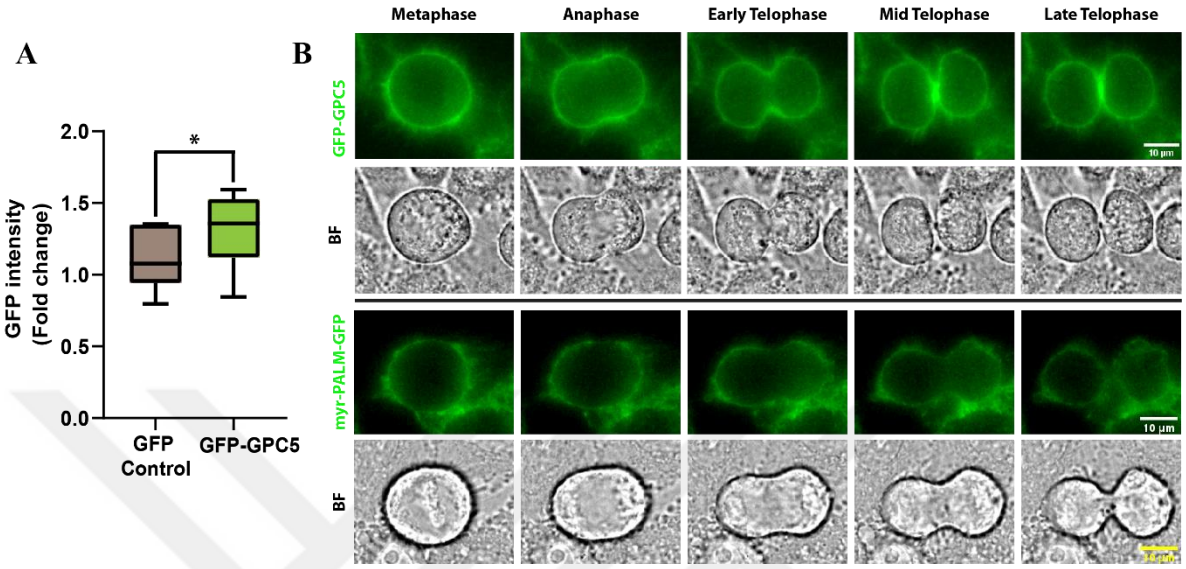

Figure 3. 1. 1: Localization of GPC5 throughout cell division.

(A) GFP intensity quantification was done by taking the intensity in between two daughter cells normalized at the mid telophase to the GFP intensity at the poles of the cells. Analysis was done using n=7 for myr-PALM-GFP Control and n=12 for the EGFP-GPC5. Unpaired Student's t test is used for the statistical significance analysis, *: p=0.0449. (**B)** Representative of the localization of EGFP-GPC5 and myr-PALM-GFP during cell division. Scale bars 10 micron.

3.2. The knock-out of GPC5 results in multinucleation.

In order to observe the effect of GPC5 on cell division, we employed an inducible GPC5 knock-out in HelaCas9 cells by editing their genome using a CRISPR/Cas9-based technology. After an induction period of 72 hours with Dox, the GPC5 knock-out efficiencies of sg2 expressing HeLaCas9 cells were analyzed by quantitative real-time PCR (Figure 3.2.1, A-left panel). In HeLaCas9 GPC5 sg2 cells, a reduction in GPC5 expression of 83% was seen in response to the induction of Dox.

The percentage of multinucleated HeLaCas9 GPC5 sg2 cells had a significant increase after GPC5 knock-out, going from 1.39 percent to 6.71 percent (Figure 3. 2.1, A). This

multinucleation phenotype was rescued in GPC5 knock-out cells by the ectopic expression of cMyc-GPC5 (CRISPR-resistant), resulting in a difference that was not statistically significant between control cells and GPC5 KO cells.

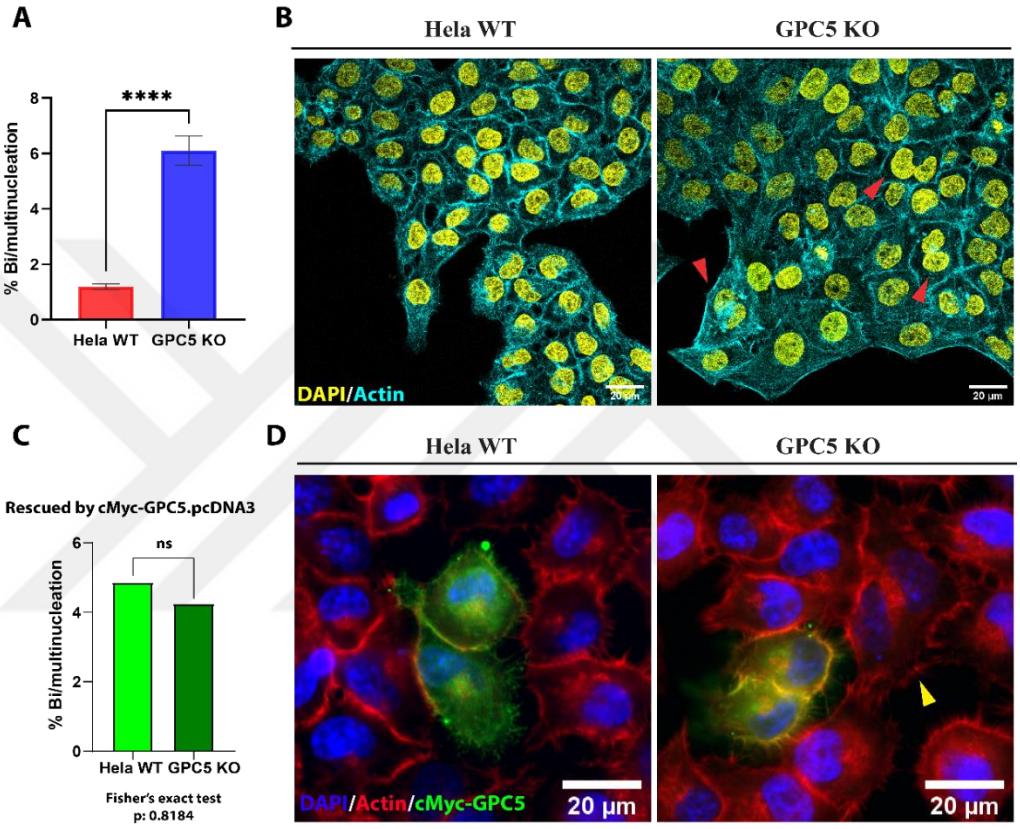

Figure 3. 2. 1: GPC5 knock-out results in multinucleation phenotype in HelaCas9 cells. **(A)** Quantification of the multinucleated cell percentage in HelaCas9 WT and HelaCas9 GPC5 KO. For the statistical analysis Unpaired Student's t-test was applied in the averages of three biological replicates, ****: <0.0001. **(B)** Representative images of HelaCas9WT and HelaCas9 GPC5 KO cells (Red arrows indicate the multinucleated cells). **(C)** Quantification of the multinucleated cell percentage in HelaCas9 WT and HelaCas9 GPC5 KO transfected with CRISPR-Resistant cMyc-GPC5 constructs (n~200). For the significance analysis Fisher's exact test with odds ratio has been performed; ns: not significant. **(D)** Representative images of HelaCas9WT and HelaCas9 GPC5 KO cells transfected with CRISPR-Resistant cMyc-GPC5 constructs (Yellow arrows indicate the multinucleated cells). Scale bars: 20 µm.

3.3. Knocking out GPC5 causes a shift in the division plane orientation.

We performed live cell imaging experiments with HelaCas9 WT and HelaCas9 GPC5 knock-out cells and explored the cell division phenotypes to define the defects in HelaCas9 GPC5 knock-out cells that led to multinucleation. HelaCas9 GPC5 KO cells were able to round up as well as control samples in all the samples; however, problems at the subsequent stages of cell division were identified.

In cells where GPC5 had been knocked out, the orientation of the division plane was altered during cytokinesis. While the daughter cells produced by the HelaCas9 WT cells are created perpendicular to the attachment surface with just 1.8 percent of them exhibiting abnormal division plane orientation, 29.7 percent of the cells produced by the HelaCas9 GPC5 KO are abnormally oriented in their division planes (Figure 3.3.1.). Almost 30% of the HelaCas9 GPC5 KO cells, one of the daughter cells have abnormality in their adhesion to the surface.

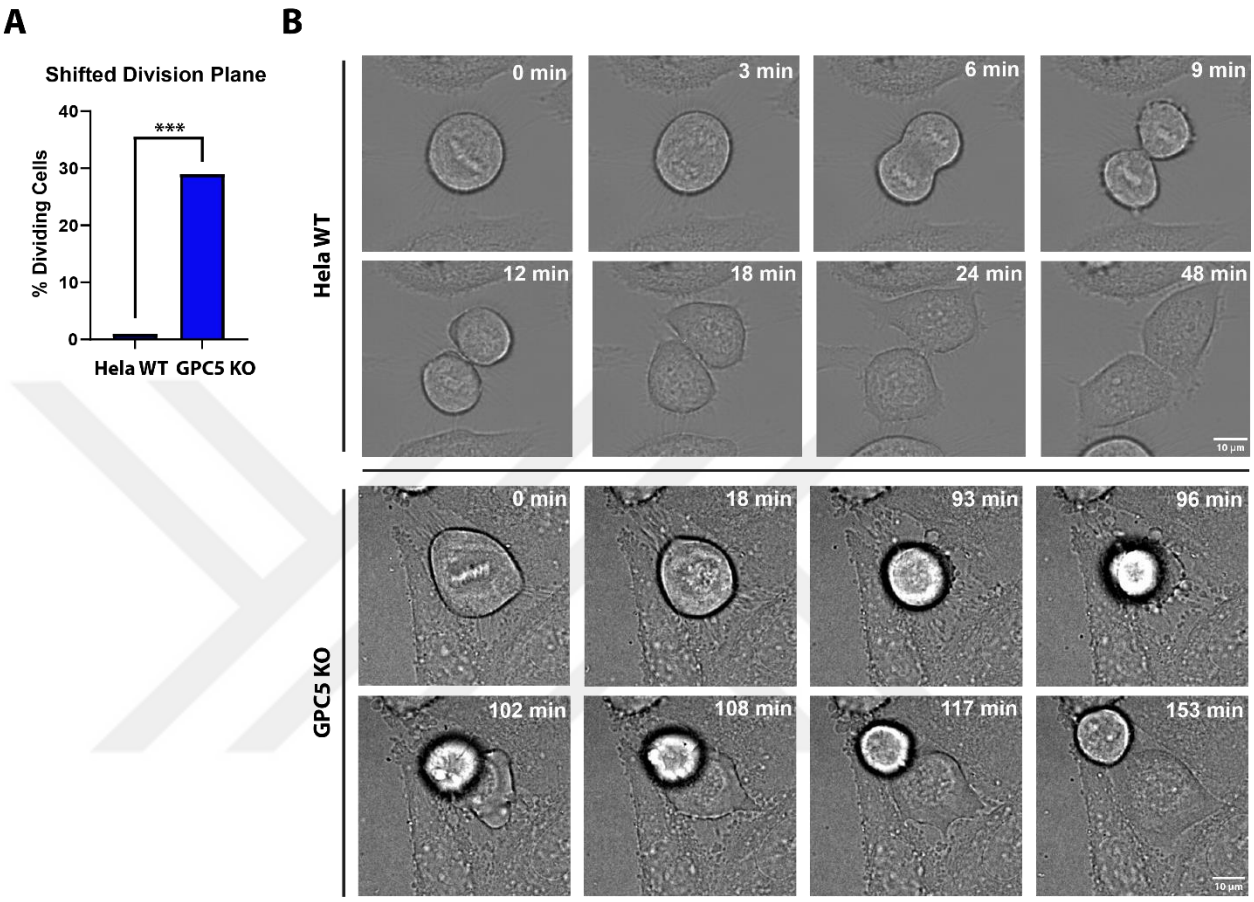

Figure 3. 3. 1: HelaCas9 GPC5 KO Cells Exhibit Shifted Cell Division Plane During Cytokinesis. (A) Quantification of the percentage of dividing cells exhibiting a shift in the orientation of the division plane in HelaCas9 WT (n=56) and HelaCas9 GPC5 KO (n=37). For the statistical analysis Fischer's Exact Test has been used. ***: p=0.0001**. (B)** Representative images of HelaCas9 WT and HelaCas9 GPC5 KO cells. Scale bar: 10 µm.

Another defect observed in the HelaCas9 GPC5 KO cells is prolonged time for the cell division. As seen in the upper panel of Figure 3.3.1, HelaCas9 GPC5 KO cells complete the division around 155 minutes while HelaCas9 WT cells complete the cytokinesis in around 50 minutes.

3.4. HelaCas9 GPC5 KO cells exhibit prolonged late cytokinesis.

To further understand the defect in cytokinesis in the absence of GPC5, we performed another analysis. In this analysis the time necessary for the mitosis, early cytokinesis and late cytokinesis was quantified in both HelaCas9 WT and HelaCas9 GPC5 KO cells. For the mitosis, time between cell rounding and metaphase were quantified. The time between metaphase to midbody formation was quantified as or the early cytokinesis. Lastly, the time interval for the late cytokinesis was recorded between the first appearance of the midbody to the completion of the cytokinesis whether successfully or not.

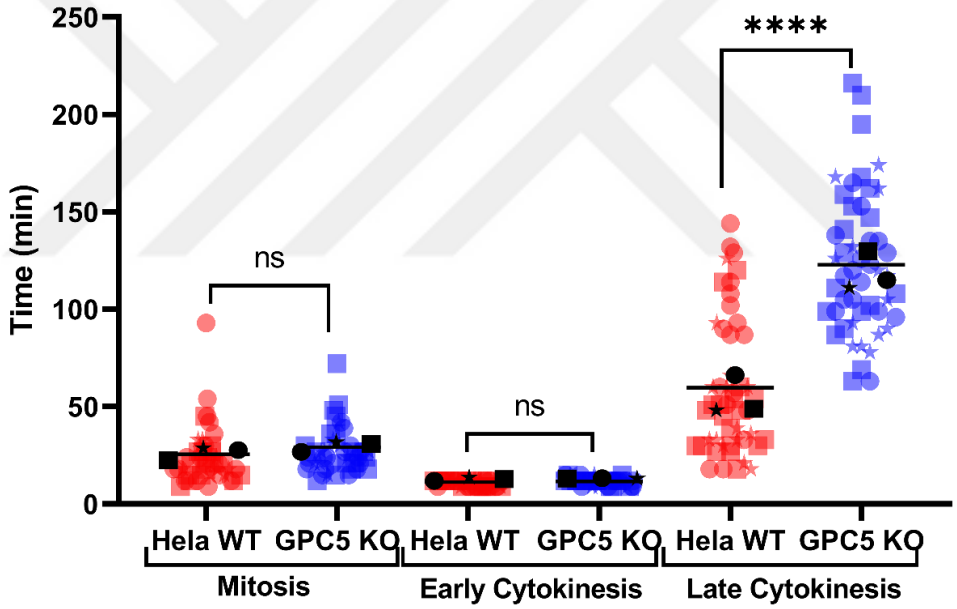

Figure 3.4.1: HelaCas9 GPC5-KO cells result in prolonged late cytokinesis. Quantification of the time for mitosis; from cell rounding to metaphase, early cytokinesis; from anaphase to midbody formation, and late cytokinesis; from midbody formation to the end of abscission. Red; HelaCAs9 WT, Blue; HelaCas9 GPC5 KO. (Circle, square and stars are representing different biological replicates; black circle, square and star shows the mean of each biological replicate (n=22)) For the statistical analysis two-way ANOVA was used; ****: < 0.0001.

As seen in the Figure 4.4., there was no significant difference between HelaCas9 WT and HelaCas9 GPC5 KO cells in terms of the time for mitosis and early cytokinesis. However, we observed that in the absence of GPC5, cells need significantly more time to be able to finish cytokinesis whether successfully or not.

3.5. GPC5 knock-out causes a delay in midbody abscission.

After we showed that HelaCas9 GPC5 KO cells causes multinucleation (Figure 4.2) and they exhibit prolonged late cytokinesis (Figure 4.4). We wanted to see whether the prolonged late cytokinesis is the cause for the multinucleation which is a cytokinesis defect phenotype. To this end, we performed brightfield live cell imaging using HelaCas9 WT and HelaCas9 GPC5 KO cells.

We observed that in the absence of GPC5, cells need more time to be able to finish the abscission. Even if the GPC5 KO cells can divide successfully they need more time for the midbody abscission. HelaCas9 WT cells finishes abscission in 50 minutes while HelaCas9 GPC5 KO cells can finish the abscission around 122 minutes whether successfully or not. In conclusion, we observe that the time for the abscission of the midbody is significantly increased in the HelaCas9 GPC5 KO cells (Figure 4. 5 and Figure 4.6).

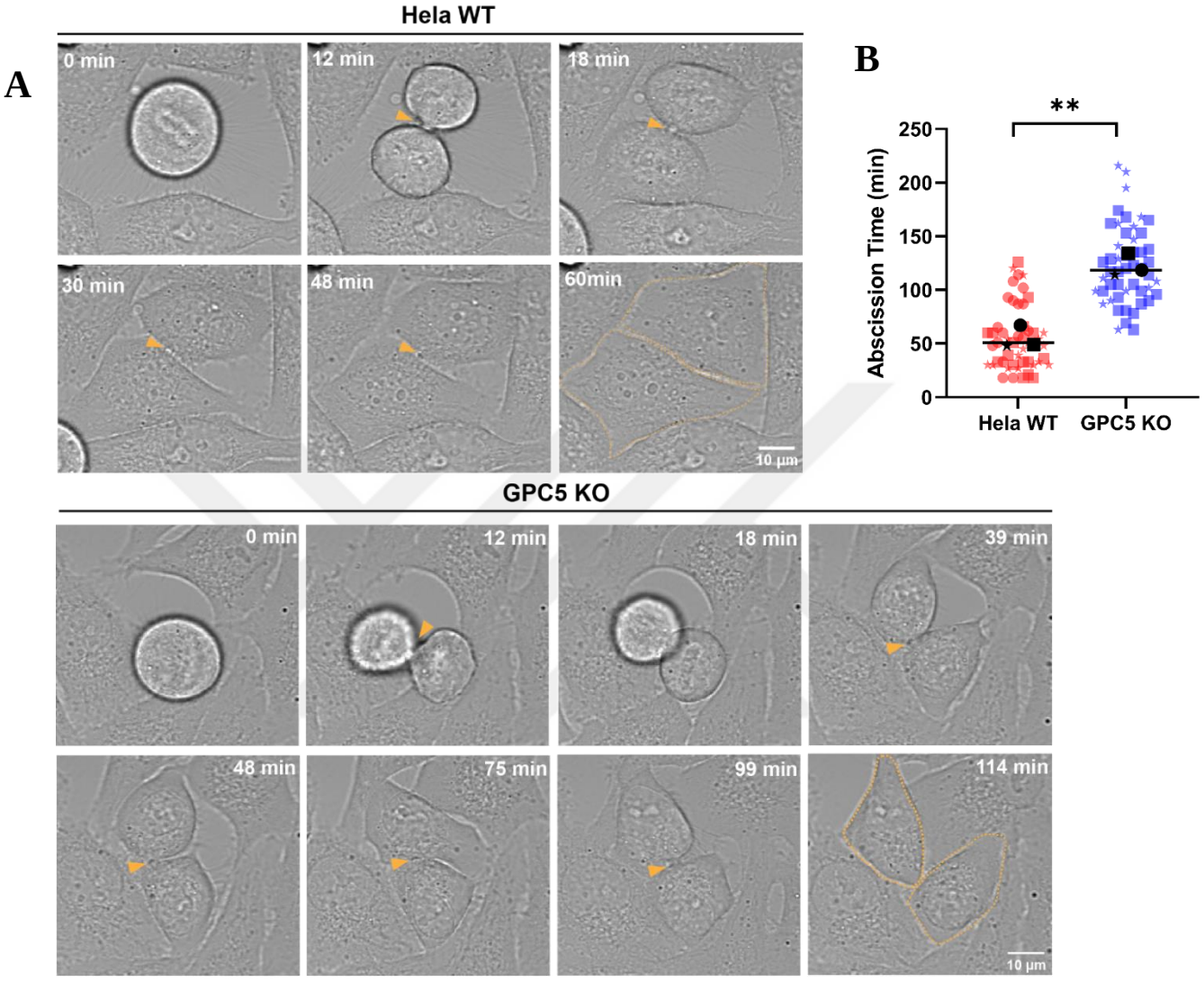

Figure 3.5.1: HelaCas9 GPC5 KO cells delay the abscission (A) Representative of the abscission time in HelaCas9 WT and GPC5 KO cells. Midbody formation step was pointed with an arrow and separated cells were shown in yellow dashed lines **(B)** Quantification of abscission time. (Red; HelaCas9 WT, Blue; HelaCas9 GPC5 KO). (Circle, square and stars are representing different biological replicates; black circle, square and star shows the mean of each biological replicate (n=17)) For the statistical analysis Unpaired Student's t-test was used; **: < 0.0014. Scale bars: 10 µm.

3.6. The abscission time delay was worsened when the integrin-mediated adhesion is interfered.

The proteins which are in the proximity of GPC5 during cytokinesis were analyzed and visualized by Ezgi Memiş and Altuğ Kamacıoğlu. Most of the proteins which were on the network clustering of the GPC5's possible interaction partners (Figure 3.6.1) have a role in cell adhesion and migration along with RhoA activation, actin reorganization, glycolysis, and others.

Since we know that GPC5 knock-out causes an abnormal division plane orientation during cytokinesis and, we know that GPC5 absence results in prolonged abscission, we thought that the reason for these phenotypes might be related with the adhesion defect caused by the GPC5 absence. Based on the proteins in the GPC5 interaction partners, we saw Integrin β1 (ITGB1) which has a role in cell adhesion, we further tried to understand the effect of the adhesion on GPC5 KO cells. We wanted to understand how the abscission will be affected when integrin mediated cell adhesion is interfered. To this end, another brightfield live cell analysis were done using a peptide called GRGDSP to be able to block all integrin-mediated adhesion in the cells.

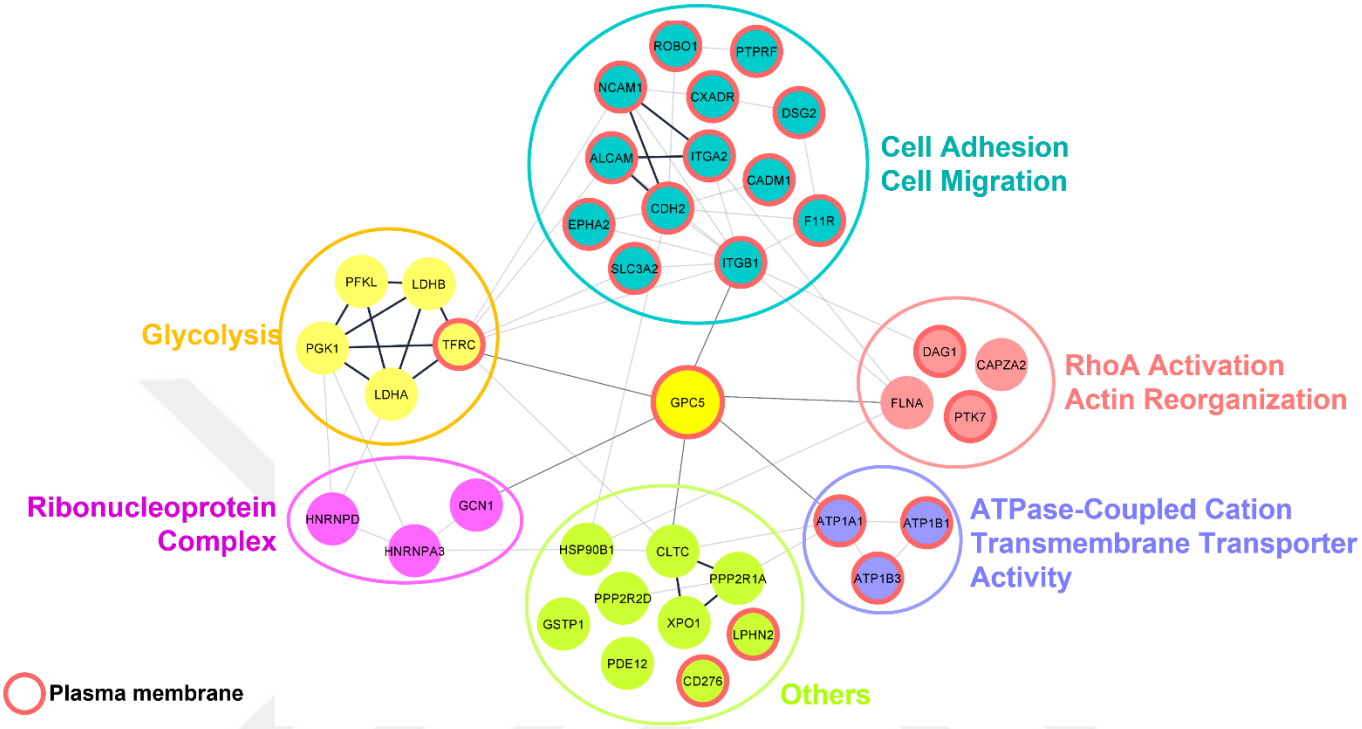

Figure 3. 6.1: Network clustering of the GPC5's cytokinesis specific interaction partners

In the presence of 1 mM GRGDSP peptide, we observed that HelaCas9 GPC5 KO cells need even more time to be able to finish abscission whether successfully or not. As seen in Figure 3.6.2, HelaCas9 GPC5 KO cells undergo abscission around 252 minutes while the HelaCas9 WT cells complete this process in around 162 minutes. When we quantified the abscission time in these cells, we again saw a significant increase (Figure 3.6.3, A). Also, when we compare the abscission time differences all together, we saw that abscission time was further prolonged when the integrin-mediated cell adhesion was blocked (Figure 3.6.3, B).

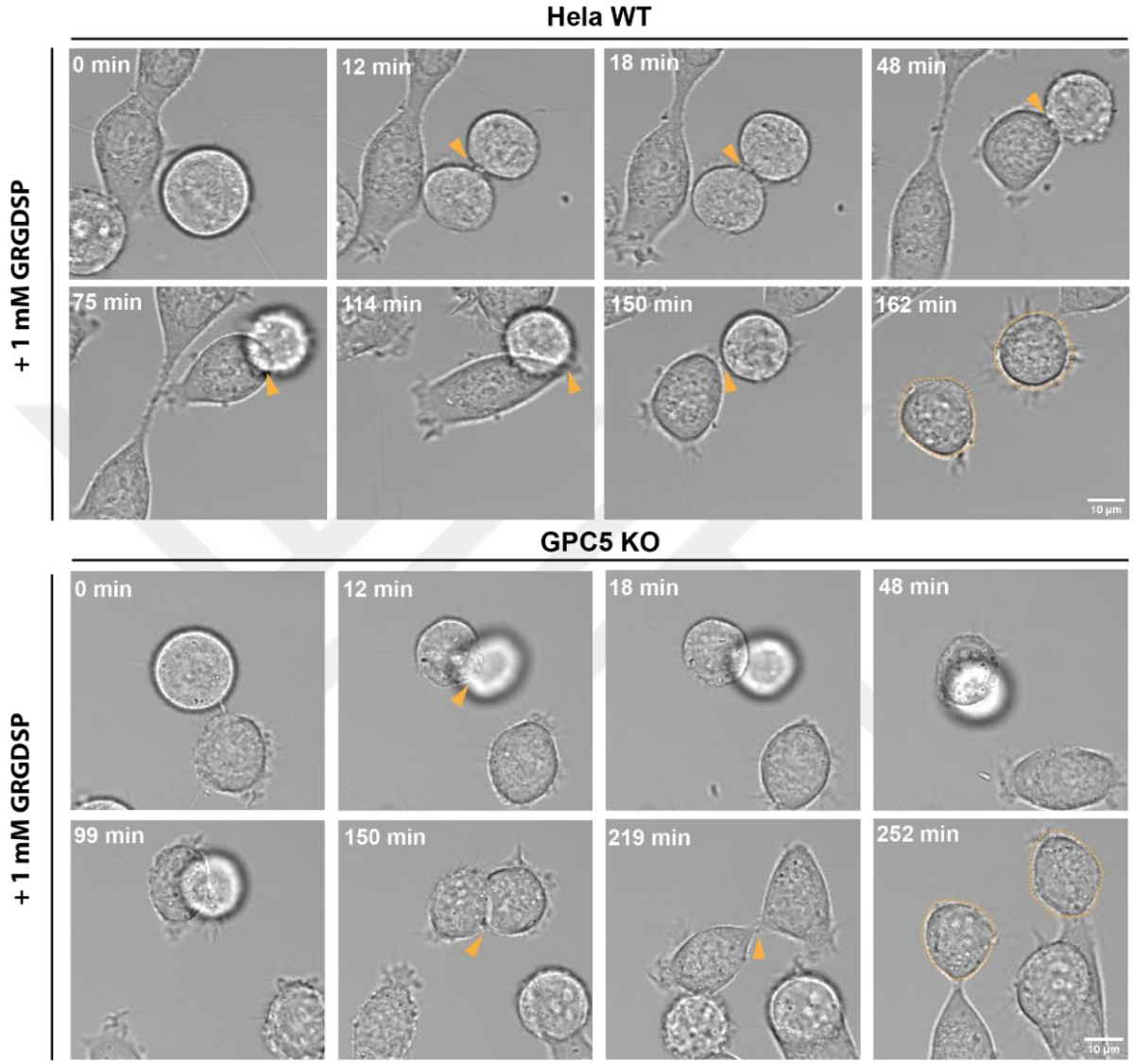

Figure 3.6.2: Representative of prolonged abscission in HelaCas9 WT and HelaCas9 GPC5 KO cells. Representative of the abscission time in HelaCas9 WT and GPC5 KO cells in the presence of 1 mM GRGDSP. Midbody formation step was pointed with an arrow and separated cells were shown in yellow dashed lines. Scale bars 10 micron.

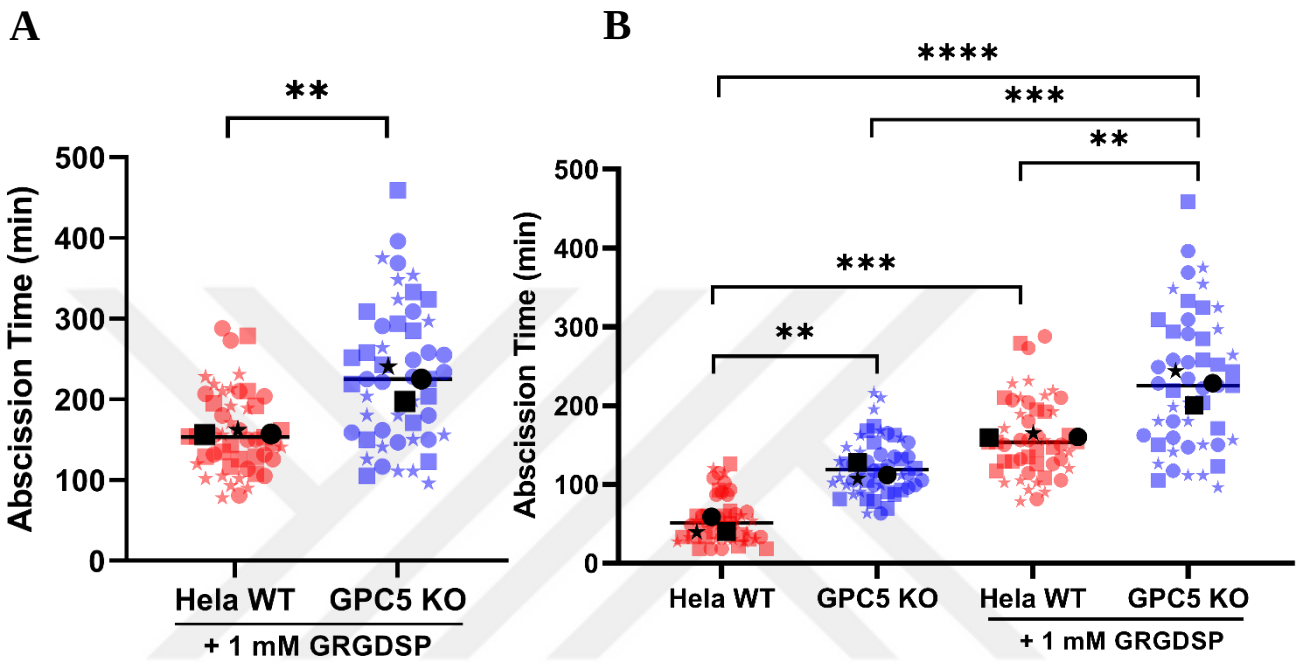

Figure 3.6.3: HelaCas9 GPC5 KO cells delay the abscission even more when integrin-mediated adhesion was blocked

(A) Quantification of abscission time. (Red; HelaCas9 WT, Blue; HelaCas9 GPC5 KO). (Circle, square and stars are representing different biological replicates; black circle, square and star shows the mean of each biological replicate (n=17)) For the statistical analysis Unpaired Student's t-test was used; **: < 0.0079. **(B)** Comparison of the abscission time of peptide treated vs. non-treated cells. For the statistical analysis two-way ANOVA was used. **: < 0.0079, ***: 0.0003, ****: <0.0001.

3.7. Prolonged abscission time can be rescued with the enhancement of the adhesion

After seen the effect of adhesion on the abscission time, we furhter investigated whether the prolonged abscission time phenotype can be rescued with the enhancement of cell adhesion with the help of coating. With this purpose a preliminary analysis of brightfield live cell imaging was done using laminin coated dishes and we observed that the abscission time difference between HelaCas9 WT and HelaCas9 GPC5 KO cells was became non significant (Figure 3.7.1). The number of the cells in each replicate was really low, so that this analysis should be done with an increase number of cells.

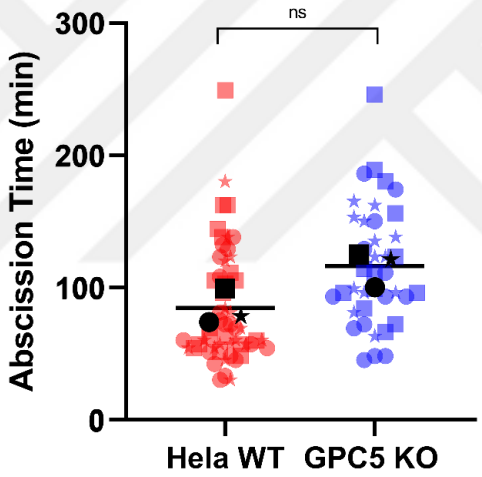

Figure 3.7.1: Quantification of the preliminary experiment for the rescue of the prolonged abscission time. Quantification of abscission time. (Red; HelaCas9 WT, Blue; HelaCas9 GPC5 KO). (Circle, square and stars are representing different biological replicates; black circle, square and star shows the mean of each biological replicate (n=8)) For the statistical analysis Mann Whitney test was used; p value = 0.1.

Next, we further investigated the effect of the enhancement of the adhesion in terms of multinucleation. By using different coating materials like Concanavalin A, laminin and PLL to understand this rescue phenotype is dependent on the laminin interaction or not. As a result, we found out that multinucleation phenotype was rescued in HelaCas9 GPC5 KO when the cell adhesion is enhanced, and it is not dependent on the coating material (Figure 3.7.2.)

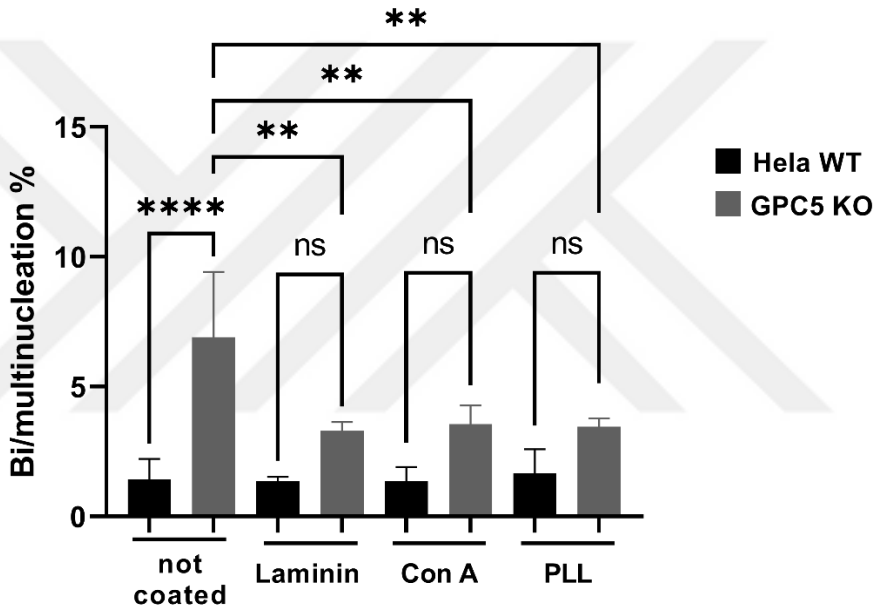

Figure 3.7.2: The multinucleation phenotype was rescued with the enhancement of the cell adhesion. Quantification of the percentage of multinucleated cell in HelaCas9 WT and HelaCas9 GPC5 KO. For the statistical analysis the average of each biological replicate (n=600) were compared with two-way ANOVA; **: 0.0047 (Laminin), **: 0.0089 (Con A), **: 0.0071 (PLL), ****: <0.0001.

3.8. The bottom ingression was significantly decreased in GPC5 knock-out cells

In order to understand the shifted division plane orientation phenotype in GPC5 KO cells, we further investigated HelaCas9 GPC5 KO cells with the help of confocal imaging. When the GPC5 is absent in the cells we saw that the bottom ingression in the cytokinetic cells were significantly decreased (Figure 3.8.1).

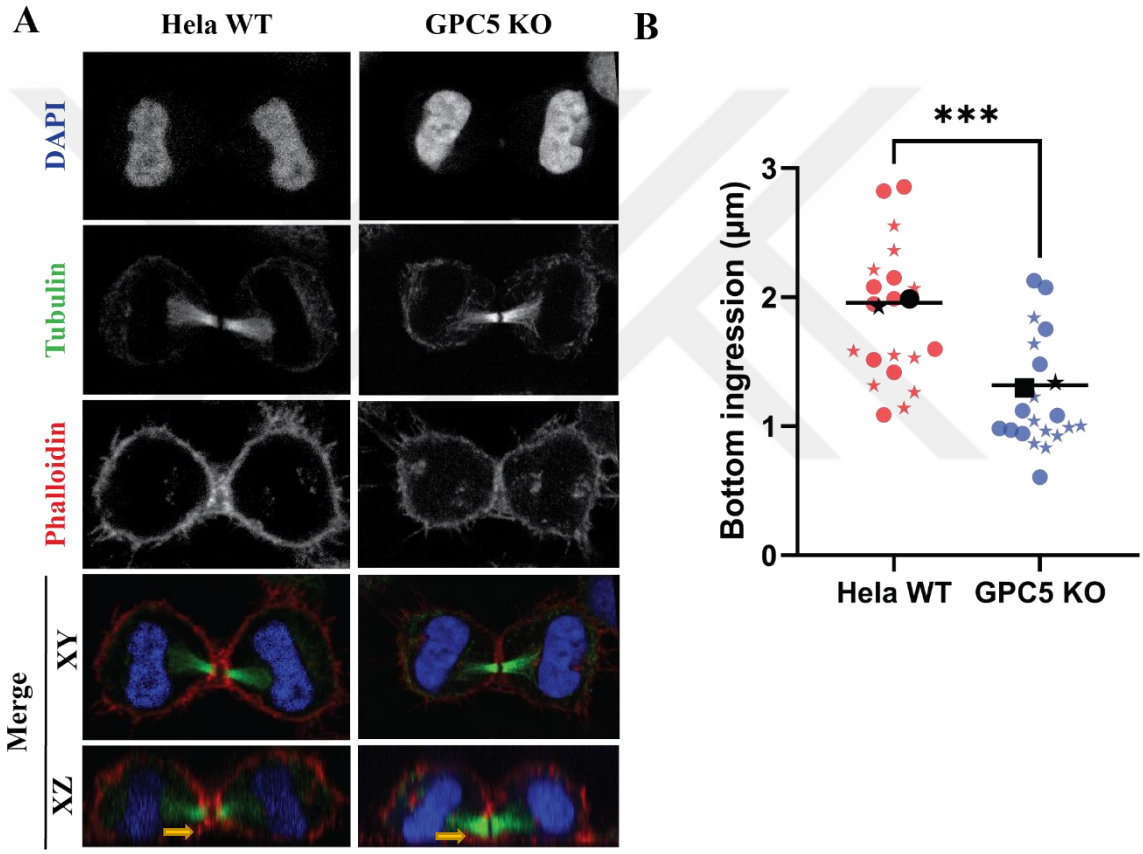

Figure 3.8.1: Bottom ingression at the intercellular bridge was significantly decreased in HelaCas9 GPC5 KO. (A) Representative images of Hela WT and GPC5 KO cells. Scale bars:10 micron. **(B)** Quantification of the bottom ingression. (Red; HelaCas9 WT, Blue; HelaCas9 GPC5 KO). (Circle and stars are representing two different biological replicates; black circle and star shows the mean of each biological replicate (n=10)). For the statistical analysis Unpaired Student's t-test was used; **: < 0.0002.

As indicated before in this section, Integrin β1 is one of the possible interaction partners of GPC5 during cytokinesis (Figure 3.6.1). Also, the bottom ingression in GPC5 KO cells were also decreased during cytokinesis (Figure 3.8.1). Using similar confocal imaging, we next compare the level of Integrin β1 in HelaCas9 WT and HelaCas9 GPC5 KO cells.

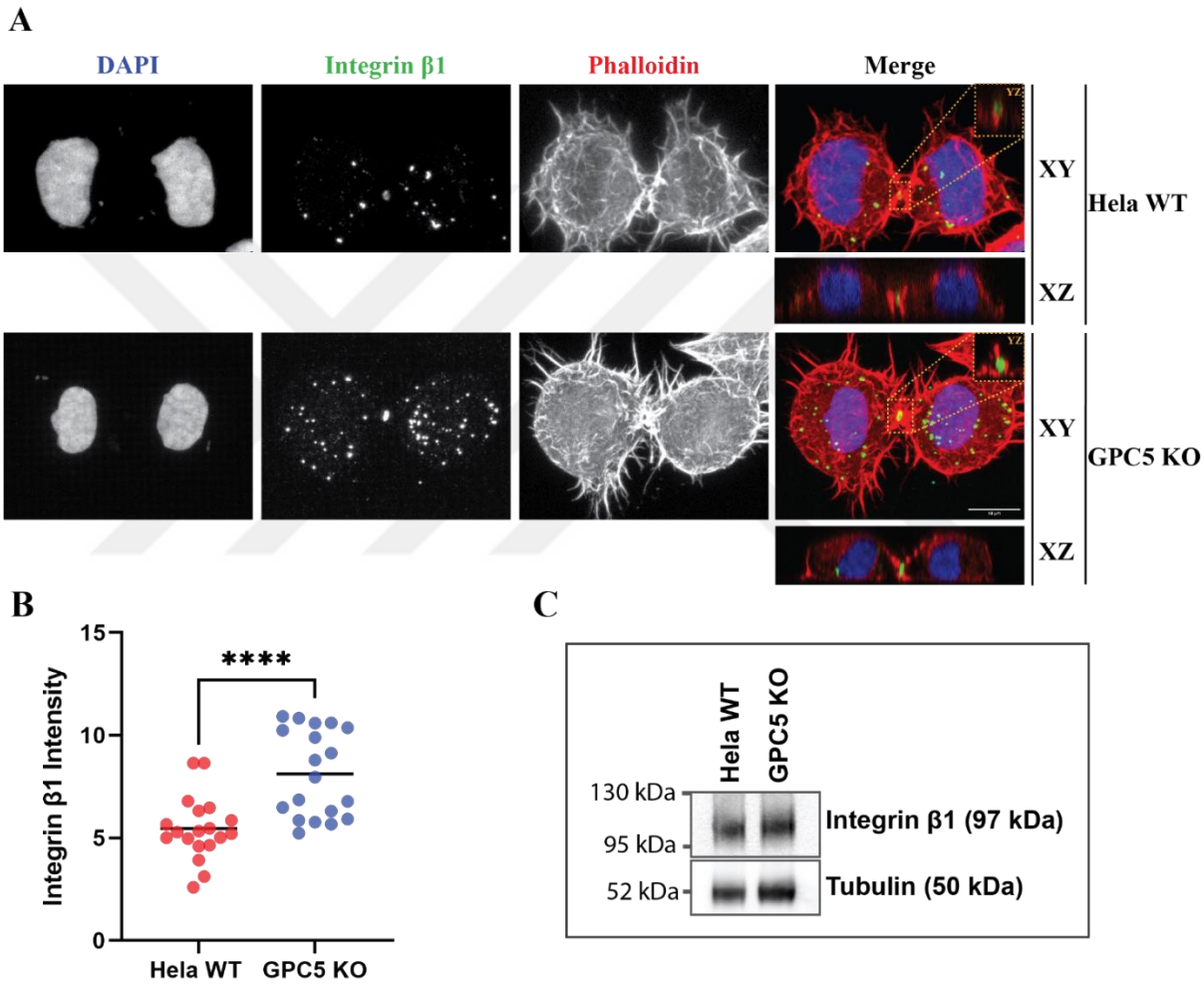

Figure 3.8.2: Integrin β1 enriches at midbody in the absence of GPC5 during cytokinesis. (A) Representative images of integrin β1 in Hela WT and GPC5 KO cells. Scale bars:10 μm. **(B)** Quantification of the integrin β1 intensity at the midbody. (Red; HelaCas9 WT, Blue; HelaCas9 GPC5 KO. For the statistical analysis Mann-Whitney test was used; ****: <0.0001. **(C)** The protein levels of integrin β1 and Tubulin in Hela WT and GPC5 KO.

The integrin β1 foci were observed throughout the cell. Also, based on the DNA staining we observed that integrin β1 was localized to the midbody during cytokinesis. As represented in Figure 3.8.1, B; GPC5 KO cells again showed a decrease in their bottom ingression levels (Figure 3.8.2, A; XZ view). Lastly, we also observed that the integrin β1 intensity was significantly increased at the midbody in the absence of GPC5 (Figure 3.8.2, B) while we did not observe any difference in the protein level of integrin β1 between WT and GPC5 KO cells (Figure 3.8.2, C).

3.9. Glypican 5 is surrounding the midbody during cytokinesis

Next, we demonstrated the localization of glypican 5 and integrin β1 during late cytokinesis at the same time. To this end we used polokinase as a midbody marker and EGFP-GPC5 for the Glypican 5 localization. As seen in the YZ image of Figure 3.9.1 Glypican 5 is surrounding the midbody during late cytokinesis. Also, we observed that Glypican 5 is located at the bottom ingression during division (Figure 3.9.1, XZ view).

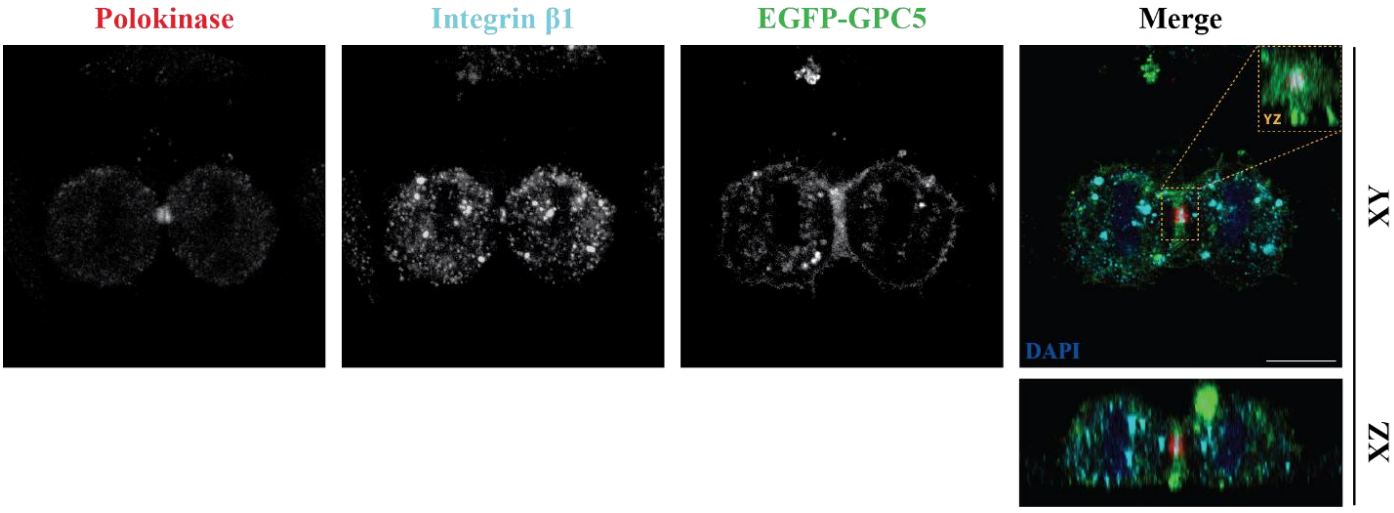

Figure 3.9.1: The localization of Glypican 5, Integrin β1 during late cytokinesis. Representative images of EGFP-GPC5; green, Integrin β1; cyan, and polokinase; red during cytokinesis. Scale bar: 10 μm.

3.10. The effect of the depletion in possible interaction partners on GPC5 knock-out cells

The network analysis was revealed that GPC5 interacting with proteins in which have a role in cell adhesion, migration, RhoA activation, and actin reorganization. Further investigations were done for the DAG1; a dystroglycan that has a role in RhoA activation and actin reorganization, and ROBO1; roundabout homolog 1 which have a role in cell adhesion and migration.

To this end we depleted the levels of DAG1 in the cells using shRNA technology. The level of DAG1 was successfully depleted using shRNA1 and shRNA3 as shown in Figure 3.10.1, A. Then, we examine the multinucleation percentage of theDAG1 depleted cells and there was significant increase in the multinucleation percentage levels in both DAG1sh1 and DAG1sh3 (Figure 3.10.1, B).

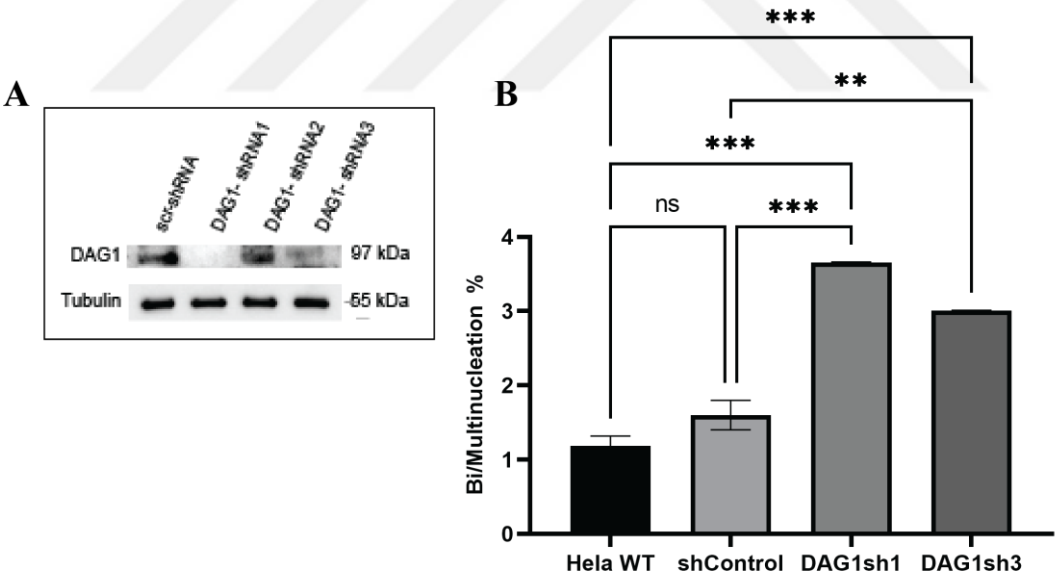

Figure 3.10.1: The effect of the depletion of DAG1 in terms of multinucleation phenotype. (A) The level of DAG1 and Tubulin in shControl and DAG1 depleted cells. **(B)** Quantification of the percentage of multinucleated cells in DAG1 depleted cells. For the statistical analysis the average of each biological replicate (n~600) were compared with one-way ANOVA; **: 0.0011, ***: <0.004.

The level of ROBO1 was also depleted in HelaCas9 WT cells using three different shRNA oligos (Figure 3.10.2, A). The multinucleation percentage of the ROBO1 depleted cells were analyzed using the fixed images of the immunostaining, and ROBO1sh1 cells were showed a significant increase as seen in Figure 3.10.2, B.

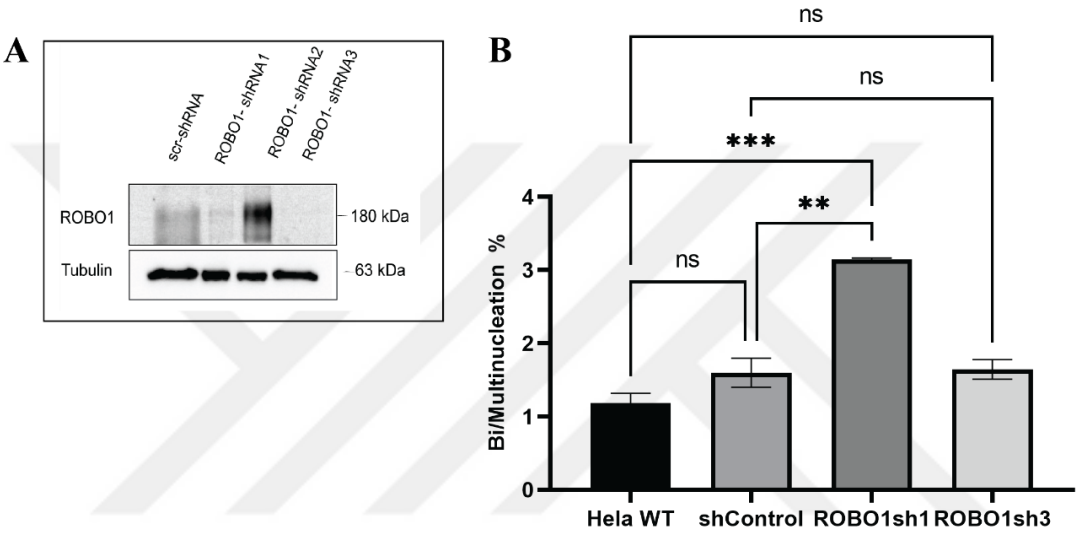

Figure 3.10.2: The effect of the depletion of ROBO1 in terms of multinucleation phenotype. (A) The level of ROBO1 and Tubulin in shControl and ROBO1 depleted cells. **(B)** Quantification of the percentage of multinucleated cells in ROBO1 depleted cells. For the statistical analysis the average of each biological replicate (n=500) were compared with one-way ANOVA; **: 0.0013, ***: 0.005.

Next, to investigate the effect on the multinucleation level of the DAG1 depletion in GPC5 KO cells, we performed another immunostaining. The depletion of the DAG1 did not affect the percentage of the multinucleation cell significantly in HelaCas9 GPC5 KO cells (Figure 3.10.3). In ROBO1sh1 cells, we observed a slight increase in the multinucleation percentage in GPC5 KO cells when we compare it to the shControl GPC5 KO cells. The increase in the multinucleation was slightly but not significantly increased when ROBO1 depleted and GPC5 knocked out.

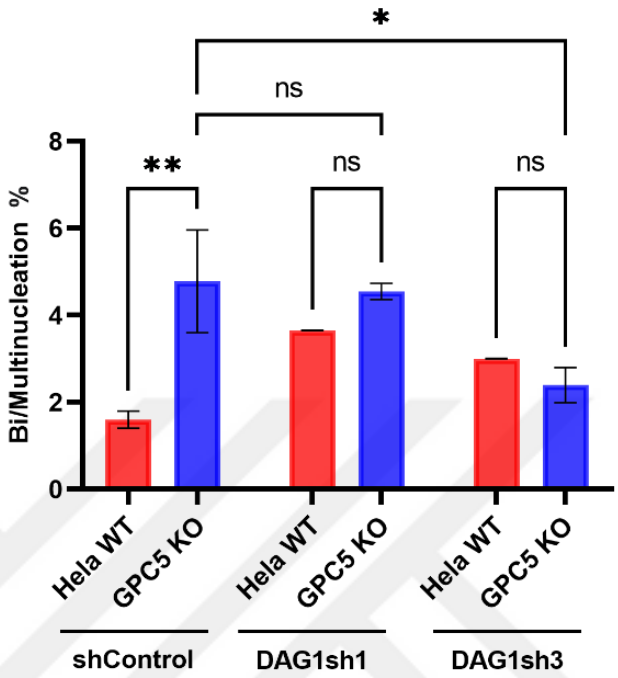

Figure 3.10.3: The depletion of DAG1 did not increase the multinucleation level. Quantification of the percentage of multinucleated cells with DAG1 depletion in HelaCas9 WT and HelaCas9 GPC5 KO cells. For the statistical analysis the average of each biological replicate (n~600) was compared with two-way ANOVA; *: 0.0268, **: 0.0067.

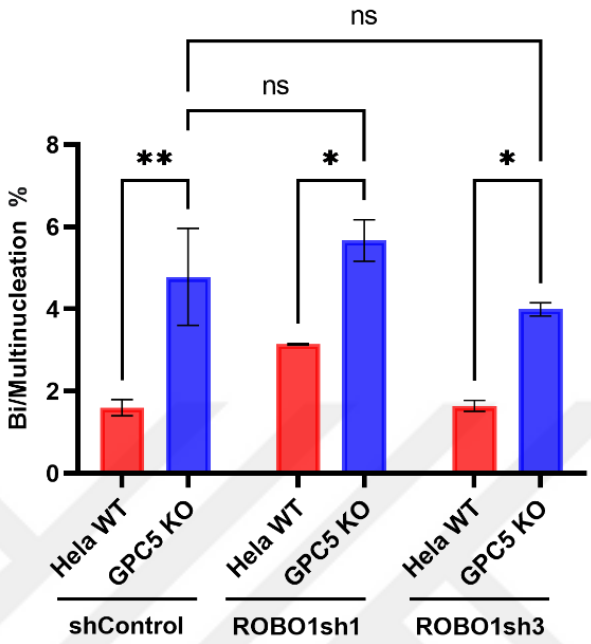

Figure 3.10.4: The depletion of ROBO1 did not affect the multinucleation level. Quantification of the percentage of multinucleated cells with ROBO1 depletion in HelaCas9 WT and HelaCas9 GPC5 KO cells. For the statistical analysis the average of each biological replicate (n~600) was compared with two-way ANOVA; *: 0.0242 (sh1), *:0.0335 (sh3), **: 0.0078.

3.11. The localization of the DAG1 and ROBO1 in HelaCas9 WT and GPC5 KO cells.

Lastly, the localization of DAG1 and ROBO1 was compared in between HelaCas9 WT and HelaCas9 GPC5 KO cells. Based on the quantifications both DAG1 and ROBO1 localization did not change (Figure 3.11.1 and Figure 3.11.2).

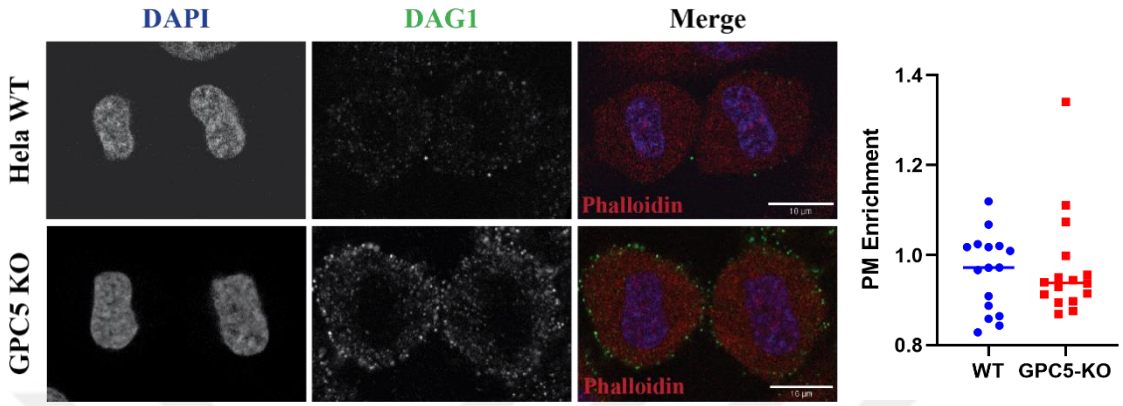

Figure 3.11.1: The localization of the DAG1 in cytokinesis. Representative images of DAG1; green, phalloidin and DAPI stained HelaCas9 WT and HelaCas9 GPC5 KO cells. Scale bar: 10 µm.

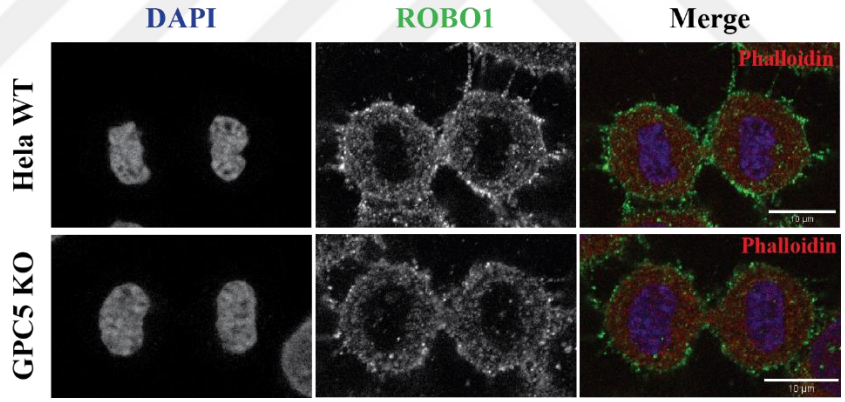

Figure 3.11.2: The localization of the ROBO1 in cytokinesis. Representative images of ROBO1; green, phalloidin and DAPI stained HelaCas9 WT and HelaCas9 GPC5 KO cells. Scale bar: 10 µm.

Chapter 4:

DISCUSSION

In this study, we illuminate the cell division role of Glypican 5 (GPC5) by performing immunofluorescence staining and live cell imaging. Also, we investigated the function of previously identified interaction partners of GPC5. We first examined the spatiotemporal localization of GPC5 throughout cell division with the help of EGFP-GPC5 transfected Hela Kyoto cells. For the control cells, we transfected Hela Kyoto cells with myr-PALM-GFP since it targets specifically to the plasma membrane through the myrosilation and palmitoylation (Zacharias, 2002). We demonstrated that GPC5 is localizing to the plasma membrane during mitosis. Based on the analysis, which we use the intensity of myr-PALM-GFP tagged cells, GPC5 significantly enriches during cytokinesis in between dividing cells.

To understand the cell division role of the glypican, we knocked out the GPC5 in doxycycline inducible CRISPR-Cas9 cells and GPC5 sgRNAs which designed by Dr. Federico Dona, Eggert Group, King's College London. Through the 72-hour induction, we observed that GPC5 levels are significantly decreased (84%). When GPC5 knocked out, we observed a significant increase in the multinucleated cell percentage from 1% to 6%. Also, the multinucleation phenotype was rescued using CRISPR-resistant c-Myc-GPC5 construct. Since GPC5 KO causes multinucleation phenotype, which is a result of the cell division failure, we conclude that GPC5 have a role in cell division.

After showing GPC5 does have a role in cell division, we performed live cell imaging in HelaCas9 WT and HelaCas9 GPC5 KO cells to understand where GPC5 function during cell division. From our live cell imaging, we observed that there is a significant increase in the percentage of dividing cells which exhibit a shift in their division plane orientation when we knock-out the GPC5. In almost 30% percent of the population, one of the dividing cells of the HelaCas9 GPC5 KO cells couldn't adhere to the surface as HelaCas9 WT cells. This suggest that in the absence of GPC5, dividing cells exhibit adhesion defects in cytokinesis.

To understand the stage of the GPC5 is functioning in the cell division, we performed another detailed analysis where we separated the cell division in 3 phases: mitosis, early and late cytokinesis. While we analyze the mitosis duration by quantifying the time from cell rounding to metaphase or early anaphase, the time between metaphase or early anaphase and midbody formation was quantified for the early cytokinesis. Lastly, for the late cytokinesis duration we quantified the time between midbody formation and end of the division whether it is successful or not. Based on the statistical analysis of the three biological replicates, we showed that the duration of the late cytokinesis was significantly increased in the absence of GPC5. However, there were no significant difference in the duration of mitosis and early cytokinesis between HelaCas9 WT and HelaCas9 GPC5 KO cells.

Our previous proximity proteomic analysis identified the interaction partners which have a role in cell adhesion, RhoA activation, and actin reorganization of the GPC5 during cytokinesis. One of the 38 possible interaction partners of GPC5 is ITGB1 which has a role in cell adhesion and cytokinesis (Chastney, 2021; Mathew, 2014). Since we observed that GPC5 absence resulted in adhesion defect in dividing cells and multinucleated cells, we investigated the relationship between ITGB1 and GPC5. To this end we perform another live cell imaging with the help of GRGDSP peptide and illuminate the effect of the cell adhesion on the abscission time delay which we observed in HelaCas9 GPC5 KO cells. GRGDSP is a peptide which inhibit the adherence of cells to the extracellular matrix by blocking the integrin binding sites. Our analyses showed that abscission time delay was worsened when the integrin-mediated adherence of the cell interfered.

Next, we aimed to rescue the abscission time delay in GPC5 KO cells with the enhancement of the cell attachment. With this purpose, we coated the dishes with laminin which is an ECM component and performed brightfield live cell imaging. As a result, the abscission time difference between HelaCas9 WT and HelaCas9 GPC5 KO cells were not significant when the cell attachment was enhanced. To further illuminate the effect of the cell attachment improvement, we analyze the percentage of the multinucleated cells which were supported by different ECM components like concanavalin A, laminin, and PLL. By using different ECM component, we also examine if there is an effect of the type of ECM component for the rescue. Regardless of the ECM component type, the multinucleation phenotype was also rescued with the enhanced attachment.

Based on the adhesion and cell division defects, we also examine the cell-surface interaction on these cells. Using confocal microscopy, we showed the orthogonal views of the HelaCas9 WT and HelaCas9 GPC5 KO cells. The orthogonal views of these cells showed that bottom ingression is significantly decreased, around 1 micron, in the absence of GPC5. We observed that daughter cells have a shift in their division plane orientation in these imaging also. With these observations, we think that the absence of GPC5 might cause a tension at the intercellular bridge and causing the delay in the abscission (Andrade, 2022). To further investigate this hypothesis, we also checked the integrin β1 localization. While there is no change in the protein level of integrin β1 in the HelaCas9 WT and HelaCas9 GPC5 KO cells, we observed that integrin β1 enriches significantly at the midbody during cytokinesis. Both the decrease in the bottom ingression and the increase in integrin β1 at cytokinesis also supported the possibility that GPC5 absence create high tension at the ICB and causes abscission time delay. This hypothesis also supported since these phenotypes were rescued with the additional support for the attachment of the daughter cells. It is possible that with the enhancement of attachment GPC5 KO cells could release the tension at the ICB and initiate the scission machinery (Andrade, 2022; Ariotti, 2014). When we examine the localization EGFP tagged GPC5 and integrin β1, we showed that GPC5 is surrounding the midbody where we used polo kinase as a midbody marker.

Lastly, we illuminate the effect of DAG1 and ROBO1 which are also proteins in the interactome analysis. Even though the depletion of DAG1 and ROBO1 causes multinucleation, we did not observe any additional effect in the multinucleated cell percentage in GPC5 KO cells. Then, we examine the localization of DAG1 and ROBO1 in both Hela WT and HelaCas9 GPC5 KO cells. While ROBO1 localization did not changed, we observed that DAG1 is localizes to the plasma membrane in cytokinesis. However, further imaging and analysis should be done to determine whether the localization of DAG1 to the plasma membrane is significant or not.

Overall, this study illuminates the mechanism of how the outside and the inner part of the cell communicates during division. The analysis revealed that GPC5 have a role in the late cytokinesis by regulating adhesion properties of dividing cells specifically during abscission. Through the interaction with Integrin beta 1 and DAG1, GPC5 have a role in the cell to ECM adhesion. Also, GPC5 might support the ICB and have a role in the initiation of the scission by helping the tension release at the midbody.

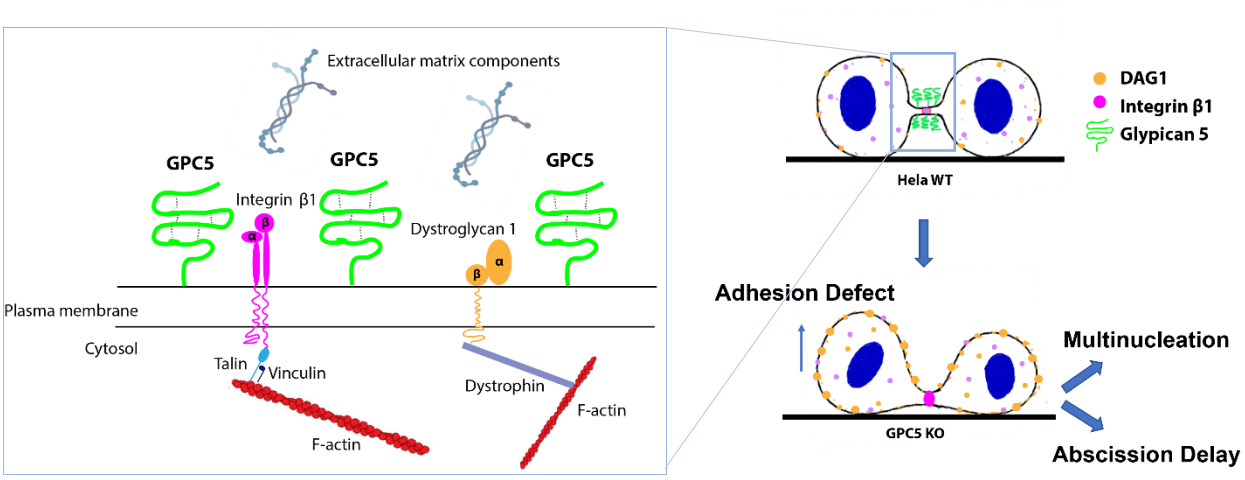

Figure 4.1. A proposed model of how GPC5 might involve in mammalian cytokinesis.

REFERENCES

Andrade, V., Bai, J., Gupta-Rossi, N., Jimenez, A. J., Delevoye, C., Lamaze, C., & Echard, A. (2022). Caveolae promote successful abscission by controlling intercellular bridge tension during cytokinesis. *Sci Adv, 8*(15), eabm5095. doi:10.1126/sciadv.abm5095

Ariotti, N., Fernández-Rojo, M. A., Zhou, Y., Hill, M. M., Rodkey, T. L., Inder, K. L., . . . Parton, R. G. (2014). Caveolae regulate the nanoscale organization of the plasma membrane to remotely control Ras signaling. *J Cell Biol, 204*(5), 777-792. doi:10.1083/jcb.201307055

Aszodi, A., Hunziker, E. B., Brakebusch, C., & Fässler, R. (2003). Beta1 integrins regulate chondrocyte rotation, G1 progression, and cytokinesis. *Genes Dev, 17*(19), 2465-2479. doi:10.1101/gad.277003

Barnum, K. J., & O'Connell, M. J. (2014). Cell cycle regulation by checkpoints. *Methods Mol Biol, 1170*, 29-40. doi:10.1007/978-1-4939-0888-2_2

Böttcher, R. T., Wiesner, S., Braun, A., Wimmer, R., Berna, A., Elad, N., . . . Fässler, R. (2009). Profilin 1 is required for abscission during late cytokinesis of chondrocytes. *Embo j, 28*(8), 1157-1169. doi:10.1038/emboj.2009.58

Breznau, E. B., Semack, A. C., Higashi, T., & Miller, A. L. (2015). MgcRacGAP restricts active RhoA at the cytokinetic furrow and both RhoA and Rac1 at cell-cell junctions in epithelial cells. *Mol Biol Cell, 26*(13), 2439-2455. doi:10.1091/mbc.E14-11-1553

Bringmann, H., & Hyman, A. A. (2005). A cytokinesis furrow is positioned by two consecutive signals. *Nature, 436*(7051), 731-734. doi:10.1038/nature03823

Burridge, K., & Chrzanowska-Wodnicka, M. (1996). Focal adhesions, contractility, and signaling. *Annu Rev Cell Dev Biol, 12*, 463-518. doi:10.1146/annurev.cellbio.12.1.463

Burton, K., & Taylor, D. L. (1997). Traction forces of cytokinesis measured with optically modified elastic substrata. *Nature, 385*(6615), 450-454. doi:10.1038/385450a0

Capurro, M., Shi, W., Izumikawa, T., Kitagawa, H., & Filmus, J. (2015). Processing by convertases is required for glypican-3-induced inhibition of Hedgehog signaling. *J Biol Chem, 290*(12), 7576-7585. doi:10.1074/jbc.M114.612705

Carvalho, A., Desai, A., & Oegema, K. (2009). Structural memory in the contractile ring makes the duration of cytokinesis independent of cell size. *Cell, 137*(5), 926-937. doi:10.1016/j.cell.2009.03.021

Caswell, P. T., & Norman, J. C. (2006). Integrin trafficking and the control of cell migration. *Traffic, 7*(1), 14-21. doi:10.1111/j.1600-0854.2005.00362.x

Caswell, P. T., Spence, H. J., Parsons, M., White, D. P., Clark, K., Cheng, K. W., . . . Norman, J. C. (2007). Rab25 associates with alpha5beta1 integrin to promote invasive migration in 3D microenvironments. *Dev Cell, 13*(4), 496-510. doi:10.1016/j.devcel.2007.08.012

Civelekoglu-Scholey, G., & Cimini, D. (2014). Modelling chromosome dynamics in mitosis: a historical perspective on models of metaphase and anaphase in eukaryotic cells. *Interface Focus, 4*(3), 20130073. doi:10.1098/rsfs.2013.0073

Dix, C. L., Matthews, H. K., Uroz, M., McLaren, S., Wolf, L., Heatley, N., . . . Baum, B. (2018). The Role of Mitotic Cell-Substrate Adhesion Re-modeling in Animal Cell Division. *Dev Cell, 45*(1), 132-145.e133. doi:10.1016/j.devcel.2018.03.009

Elia, N., Fabrikant, G., Kozlov, M. M., & Lippincott-Schwartz, J. (2012). Computational model of cytokinetic abscission driven by ESCRT-III polymerization and remodeling. *Biophys J, 102*(10), 2309-2320. doi:10.1016/j.bpj.2012.04.007

Fico, A., Maina, F., & Dono, R. (2011). Fine-tuning of cell signaling by glypicans. *Cell Mol Life Sci, 68*(6), 923-929. doi:10.1007/s00018-007-7471-6

Filmus, J., & Capurro, M. (2014). The role of glypicans in Hedgehog signaling. *Matrix Biol, 35*, 248-252. doi:10.1016/j.matbio.2013.12.007

Fujiwara, T., Bandi, M., Nitta, M., Ivanova, E. V., Bronson, R. T., & Pellman, D. (2005). Cytokinesis failure generating tetraploids promotes tumorigenesis in p53-null cells. *Nature, 437*(7061), 1043-1047. doi:10.1038/nature04217

Galipeau, P. C., Cowan, D. S., Sanchez, C. A., Barrett, M. T., Emond, M. J., Levine, D. S., . . . Reid, B. J. (1996). 17p (p53) allelic losses, 4N (G2/tetraploid) populations, and progression to aneuploidy in Barrett's esophagus. *Proc Natl Acad Sci U S A, 93*(14), 7081-7084. doi:10.1073/pnas.93.14.7081

Glotzer, M. (2005). The molecular requirements for cytokinesis. *Science, 307*(5716), 1735-1739. doi:10.1126/science.1096896

Green, R. A., Paluch, E., & Oegema, K. (2012). Cytokinesis in animal cells. *Annu Rev Cell Dev Biol, 28*, 29-58. doi:10.1146/annurev-cellbio-101011-155718

Guizetti, J., Schermelleh, L., Mäntler, J., Maar, S., Poser, I., Leonhardt, H., . . . Gerlich, D. W. (2011). Cortical constriction during abscission involves helices of ESCRT-III-dependent filaments. *Science, 331*(6024), 1616-1620. doi:10.1126/science.1201847

Högnäs, G., Tuomi, S., Veltel, S., Mattila, E., Murumägi, A., Edgren, H., . . . Ivaska, J. (2012). Cytokinesis failure due to derailed integrin traffic induces aneuploidy and oncogenic transformation in vitro and in vivo. *Oncogene, 31*(31), 3597-3606. doi:10.1038/onc.2011.527

Hong, X., Zhang, Z., Pan, L., Ma, W., Zhai, X., Gu, C., . . . Liu, Z. (2019). MicroRNA-301b promotes the proliferation and invasion of glioma cells through enhancing activation of Wnt/β-catenin signaling via targeting Glypican-5. *Eur J Pharmacol, 854*, 39-47. doi:10.1016/j.ejphar.2019.03.057

Horton, E. R., Byron, A., Askari, J. A., Ng, D. H. J., Millon-Frémillon, A., Robertson, J., . . . Humphries, M. J. (2015). Definition of a consensus integrin adhesome and its dynamics during adhesion complex assembly and disassembly. *Nat Cell Biol, 17*(12), 1577-1587. doi:10.1038/ncb3257

Hunt, T., Nasmyth, K., & Novák, B. (2011). The cell cycle. *Philos Trans R Soc Lond B Biol Sci, 366*(1584), 3494-3497. doi:10.1098/rstb.2011.0274

Iannantuono, N. V. G., & Emery, G. (2021). Rab11FIP1 maintains Rab35 at the intercellular bridge to promote actin removal and abscission. *J Cell Sci, 134*(12). doi:10.1242/jcs.244384

Johnson, D. G., & Walker, C. L. (1999). Cyclins and cell cycle checkpoints. *Annu Rev Pharmacol Toxicol, 39*, 295-312. doi:10.1146/annurev.pharmtox.39.1.295

Jones, M. C., Askari, J. A., Humphries, J. D., & Humphries, M. J. (2018). Cell adhesion is regulated by CDK1 during the cell cycle. *J Cell Biol, 217*(9), 3203-3218. doi:10.1083/jcb.201802088

Jones, M. C., Zha, J., & Humphries, M. J. (2019). Connections between the cell cycle, cell adhesion and the cytoskeleton. *Philos Trans R Soc Lond B Biol Sci, 374*(1779), 20180227. doi:10.1098/rstb.2018.0227

Kaur, S. P., & Cummings, B. S. (2019). Role of glypicans in regulation of the tumor microenvironment and cancer progression. *Biochem Pharmacol, 168*, 108-118. doi:10.1016/j.bcp.2019.06.020

Kittler, R., Pelletier, L., Heninger, A. K., Slabicki, M., Theis, M., Miroslaw, L., . . . Buchholz, F. (2007). Genome-scale RNAi profiling of cell division in human tissue culture cells. *Nat Cell Biol, 9*(12), 1401-1412. doi:10.1038/ncb1659

Kunda, P., Pelling, A. E., Liu, T., & Baum, B. (2008). Moesin controls cortical rigidity, cell rounding, and spindle morphogenesis during mitosis. *Curr Biol, 18*(2), 91-101. doi:10.1016/j.cub.2007.12.051

Lafaurie-Janvore, J., Maiuri, P., Wang, I., Pinot, M., Manneville, J. B., Betz, T., . . . Piel, M. (2013). ESCRT-III assembly and cytokinetic abscission are induced by tension release in the intercellular bridge. *Science, 339*(6127), 1625-1629. doi:10.1126/science.1233866

Lekomtsev, S., Su, K. C., Pye, V. E., Blight, K., Sundaramoorthy, S., Takaki, T., . . . Petronczki, M. (2012). Centralspindlin links the mitotic spindle to the plasma membrane during cytokinesis. *Nature, 492*(7428), 276-279. doi:10.1038/nature11773

Li, N., Gao, W., Zhang, Y. F., & Ho, M. (2018). Glypicans as Cancer Therapeutic Targets. *Trends Cancer, 4*(11), 741-754. doi:10.1016/j.trecan.2018.09.004

Li, N., Spetz, M. R., & Ho, M. (2020). The Role of Glypicans in Cancer Progression and Therapy. *J Histochem Cytochem, 68*(12), 841-862. doi:10.1369/0022155420933709

Li, Y., Sheu, C. C., Ye, Y., de Andrade, M., Wang, L., Chang, S. C., . . . Yang, P. (2010). Genetic variants and risk of lung cancer in never smokers: a genome-wide association study. *Lancet Oncol, 11*(4), 321-330. doi:10.1016/s1470-2045(10)70042-5

Lock, J. G., Jones, M. C., Askari, J. A., Gong, X., Oddone, A., Olofsson, H., . . . Strömblad, S. (2018). Reticular adhesions are a distinct class of cell-matrix adhesions that mediate attachment during mitosis. *Nat Cell Biol, 20*(11), 1290-1302. doi:10.1038/s41556-018-0220-2

Lv, L., Zhang, T., Yi, Q., Huang, Y., Wang, Z., Hou, H., . . . Shi, Q. (2012). Tetraploid cells from cytokinesis failure induce aneuploidy and spontaneous transformation of mouse ovarian surface epithelial cells. *Cell Cycle, 11*(15), 2864-2875. doi:10.4161/cc.21196

Maddox, A. S., & Burridge, K. (2003). RhoA is required for cortical retraction and rigidity during mitotic cell rounding. *J Cell Biol, 160*(2), 255-265. doi:10.1083/jcb.200207130

Mathew, S. S., Nieves, B., Sequeira, S., Sambandamoorthy, S., Pumiglia, K., Larsen, M., & Laflamme, S. E. (2014). Integrins promote cytokinesis through the RSK signaling axis. *J Cell Sci, 127*(Pt 3), 534-545. doi:10.1242/jcs.133280

Matthews, H. K., Bertoli, C., & de Bruin, R. A. M. (2022). Cell cycle control in cancer. *Nat Rev Mol Cell Biol, 23*(1), 74-88. doi:10.1038/s41580-021-00404-3

McCullough, J., Colf, L. A., & Sundquist, W. I. (2013). Membrane fission reactions of the mammalian ESCRT pathway. *Annu Rev Biochem, 82*, 663-692. doi:10.1146/annurev-biochem-072909-101058

Mierzwa, B., & Gerlich, D. W. (2014). Cytokinetic abscission: molecular mechanisms and temporal control. *Dev Cell, 31*(5), 525-538. doi:10.1016/j.devcel.2014.11.006

Nishida, T., & Kataoka, H. (2019). Glypican 3-Targeted Therapy in Hepatocellular Carcinoma. *Cancers (Basel), 11*(9). doi:10.3390/cancers11091339

Nishimura, R., Takita, J., Sato-Otsubo, A., Kato, M., Koh, K., Hanada, R., . . . Ogawa, S. (2013). Characterization of genetic lesions in rhabdomyosarcoma using a high-density single nucleotide polymorphism array. *Cancer Sci, 104*(7), 856-864. doi:10.1111/cas.12173

Normand, G., & King, R. W. (2010). Understanding cytokinesis failure. *Adv Exp Med Biol, 676*, 27-55. doi:10.1007/978-1-4419-6199-0_3

Ong, J. Y., & Torres, J. Z. (2019). Dissecting the mechanisms of cell division. *J Biol Chem, 294*(30), 11382-11390. doi:10.1074/jbc.AW119.008149

Parton, R. G., Tillu, V., McMahon, K. A., & Collins, B. M. (2021). Key phases in the formation of caveolae. *Curr Opin Cell Biol, 71*, 7-14. doi:10.1016/j.ceb.2021.01.009

Pavletich, N. P. (1999). Mechanisms of cyclin-dependent kinase regulation: structures of Cdks, their cyclin activators, and Cip and INK4 inhibitors. *J Mol Biol, 287*(5), 821-828. doi:10.1006/jmbi.1999.2640

Pellinen, T., Tuomi, S., Arjonen, A., Wolf, M., Edgren, H., Meyer, H., . . . Ivaska, J. (2008). Integrin trafficking regulated by Rab21 is necessary for cytokinesis. *Dev Cell, 15*(3), 371-385. doi:10.1016/j.devcel.2008.08.001

Peters, J. M. (2006). The anaphase promoting complex/cyclosome: a machine designed to destroy. *Nat Rev Mol Cell Biol, 7*(9), 644-656. doi:10.1038/nrm1988

Petridou, N. I., & Skourides, P. A. (2016). A ligand-independent integrin β1 mechanosensory complex guides spindle orientation. *Nat Commun, 7*, 10899. doi:10.1038/ncomms10899

Pollard, T. D., & O'Shaughnessy, B. (2019). Molecular Mechanism of Cytokinesis. *Annu Rev Biochem, 88*, 661-689. doi:10.1146/annurev-biochem-062917-012530

Ramanathan, S. P., Helenius, J., Stewart, M. P., Cattin, C. J., Hyman, A. A., & Muller, D. J. (2015). Cdk1-dependent mitotic enrichment of cortical myosin II promotes cell rounding against confinement. *Nat Cell Biol, 17*(2), 148-159. doi:10.1038/ncb3098

Reverte, C. G., Benware, A., Jones, C. W., & LaFlamme, S. E. (2006). Perturbing integrin function inhibits microtubule growth from centrosomes, spindle assembly, and cytokinesis. *J Cell Biol, 174*(4), 491-497. doi:10.1083/jcb.200603069

Sambandamoorthy, S., Mathew-Steiner, S., Varney, S., Zuidema, J. M., Gilbert, R. J., Van De Water, L., & LaFlamme, S. E. (2015). Matrix compliance and the regulation of cytokinesis. *Biol Open, 4*(7), 885-892. doi:10.1242/bio.011825

Saunders, S., Paine-Saunders, S., & Lander, A. D. (1997). Expression of the cell surface proteoglycan glypican-5 is developmentally regulated in kidney, limb, and brain. *Dev Biol, 190*(1), 78-93. doi:10.1006/dbio.1997.8690

Schafer, K. A. (1998). The cell cycle: a review. *Vet Pathol, 35*(6), 461-478. doi:10.1177/030098589803500601

Schroeder, T. E. (1972). The contractile ring. II. Determining its brief existence, volumetric changes, and vital role in cleaving Arbacia eggs. *J Cell Biol, 53*(2), 419-434. doi:10.1083/jcb.53.2.419

Song, H. H., & Filmus, J. (2002). The role of glypicans in mammalian development. *Biochim Biophys Acta, 1573*(3), 241-246. doi:10.1016/s0304-4165(02)00390-2

Streuli, C. H. (2009). Integrins and cell-fate determination. *J Cell Sci, 122*(Pt 2), 171-177. doi:10.1242/jcs.018945

Taneja, N., Fenix, A. M., Rathbun, L., Millis, B. A., Tyska, M. J., Hehnly, H., & Burnette, D. T. (2016). Focal adhesions control cleavage furrow shape and spindle tilt during mitosis. *Sci Rep, 6*, 29846. doi:10.1038/srep29846

Théry, M., & Bornens, M. (2008). Get round and stiff for mitosis. *Hfsp j, 2*(2), 65-71. doi:10.2976/1.2895661

Théry, M., Racine, V., Pépin, A., Piel, M., Chen, Y., Sibarita, J. B., & Bornens, M. (2005). The extracellular matrix guides the orientation of the cell division axis. *Nat Cell Biol, 7*(10), 947-953. doi:10.1038/ncb1307

Thullberg, M., Gad, A., Le Guyader, S., & Strömblad, S. (2007). Oncogenic H-Ras V12 promotes anchorage-independent cytokinesis in human fibroblasts. *Proc Natl Acad Sci U S A, 104*(51), 20338-20343. doi:10.1073/pnas.0706609105

Traister, A., Shi, W., & Filmus, J. (2008). Mammalian Notum induces the release of glypicans and other GPI-anchored proteins from the cell surface. *Biochem J, 410*(3), 503-511. doi:10.1042/bj20070511

Ubersax, J. A., Woodbury, E. L., Quang, P. N., Paraz, M., Blethrow, J. D., Shah, K., . . . Morgan, D. O. (2003). Targets of the cyclin-dependent kinase Cdk1. *Nature, 425*(6960), 859-864. doi:10.1038/nature02062

Uroz, M., Wistorf, S., Serra-Picamal, X., Conte, V., Sales-Pardo, M., Roca-Cusachs, P., . . . Trepat, X. (2018). Regulation of cell cycle progression by cell-cell and cell-matrix forces. *Nat Cell Biol, 20*(6), 646-654. doi:10.1038/s41556-018-0107-2

Vermeulen, K., Van Bockstaele, D. R., & Berneman, Z. N. (2003). The cell cycle: a review of regulation, deregulation and therapeutic targets in cancer. *Cell Prolif, 36*(3), 131-149. doi:10.1046/j.1365-2184.2003.00266.x

Veugelers, M., Vermeesch, J., Reekmans, G., Steinfeld, R., Marynen, P., & David, G. (1997). Characterization of glypican-5 and chromosomal localization of human GPC5, a new member of the glypican gene family. *Genomics, 40*(1), 24-30. doi:10.1006/geno.1996.4518

Vianay, B., Senger, F., Alamos, S., Anjur-Dietrich, M., Bearce, E., Cheeseman, B., . . . Théry, M. (2018). Variation in traction forces during cell cycle progression. *Biol Cell, 110*(4), 91-96. doi:10.1111/boc.201800006

Yang, X., Zhang, Z., Qiu, M., Hu, J., Fan, X., Wang, J., . . . Yin, R. (2013). Glypican-5 is a novel metastasis suppressor gene in non-small cell lung cancer. *Cancer Lett, 341*(2), 265-273. doi:10.1016/j.canlet.2013.08.020

Yuan, S., Yu, Z., Liu, Q., Zhang, M., Xiang, Y., Wu, N., . . . Li, Y. (2016). GPC5, a novel epigenetically silenced tumor suppressor, inhibits tumor growth by suppressing Wnt/β-catenin signaling in lung adenocarcinoma. *Oncogene, 35*(47), 6120-6131. doi:10.1038/onc.2016.149

Zhang, C., Liu, Z., Wang, L., Qiao, B., Du, E., Li, L., . . . Zhang, Z. (2016). Prognostic significance of GPC5 expression in patients with prostate cancer. *Tumour Biol, 37*(5), 6413-6418. doi:10.1007/s13277-015-4499-3

Zhang, C., Zhang, S., Zhang, D., Zhang, Z., Xu, Y., & Liu, S. (2011). A lung cancer gene GPC5 could also be crucial in breast cancer. *Mol Genet Metab, 103*(1), 104-105. doi:10.1016/j.ymgme.2011.02.005

Zhang, Y., Wang, J., Dong, F., Li, H., & Hou, Y. (2014). The role of GPC5 in lung metastasis of salivary adenoid cystic carcinoma. *Arch Oral Biol, 59*(11), 1172-1182. doi:10.1016/j.archoralbio.2014.07.009